



**Air-Conditioning, Heating and
Refrigeration Technology Institute**

Final Report

AHRTI Report No. 09006
JOINING TECHNIQUES ASSESSMENT

Final Report

March 2014

Denis CLODIC, Yingzhong YU
with the cooperation of ARMINES CES

EReIE
3, rue de la Croix Martre – 91120 PALAISEAU, France

Prepared for

AIR-CONDITIONING, HEATING AND REFRIGERATION TECHNOLOGY INSTITUTE,
INC
2111 Wilson Boulevard, Suite 500, Arlington, Virginia 22201-3001

DISCLAIMER

This report was prepared as an account of work sponsored by the Air-Conditioning, Heating and Refrigeration Technology Institute, Inc. (AHRTI). Neither AHRTI, its research program financial supporters, or any agency thereof, nor any of their employees, contractors, subcontractors or employees thereof - makes any warranty, expressed or implied; assumes any legal liability or responsibility for the accuracy, completeness, any third party's use of, or the results of such use of any information, apparatus, product, or process disclosed in this report; or represents that its use would not infringe privately owned rights. Reference herein to any specific commercial product, process, or service by trade name, trademark, manufacturer, or otherwise, does not necessarily constitute nor imply its endorsement, recommendation, or favoring by AHRTI, its sponsors, or any agency thereof or their contractors or subcontractors. The views and opinions of authors expressed herein do not necessarily state or reflect those of AHRTI, its program sponsors, or any agency thereof.

Funding for this project was provided by (listed alphabetically):

- Air-Conditioning, Heating and Refrigeration Institute (AHRI)
- Copper Development Association (CDA)

SUMMARY

1	Background of the research program	5
2	Literature review on Commercial Refrigeration equipment.....	5
2.1	Commercial refrigeration equipment	5
2.1.1	Stand-alone equipment.....	5
2.1.2	Condensing units	6
2.1.3	Supermarket refrigeration systems.....	6
2.2	Leakage assessment based on literature	7
2.3	Description of commonly used components and identification of their joining techniques..	9
2.3.1	Thermo expansion valves	10
2.3.2	Manual service valves.....	10
2.3.3	Solenoid valve.....	12
2.3.4	Manual shut-off valve.....	13
2.3.5	Ball valves	13
2.3.6	Pressure switches	13
2.3.7	Pressure relief valve	15
2.3.8	Schrader valve	15
2.3.9	Sight glasses.....	16
2.3.10	Filters	16
2.3.11	Flare fittings.....	17
2.3.12	Heat exchangers (evaporator and condenser).....	19
2.3.13	Brazed joint.....	19
2.4	Leak detection method review for air-conditioning and refrigeration systems	21
2.4.1	Leak detection methods.....	21
2.4.2	Concentration accumulation measurement principles.....	24
3	Leak flow rate (LFR) measurement method.....	30
3.1	Testing method based on concentration accumulation	30
3.2	Testing protocol.....	30
3.3	Test benches for systems and components	33
3.3.1	Description of the system test bench.....	34
3.3.2	Description of the component test bench	34
3.3.3	Investigation of a new charging method.....	35
4	Leak flow rate tests results.....	37
4.1	Schrader valve	38
4.2	Solenoid valves	38
4.3	Flare fittings.....	41
4.4	Ball valves	42

4.5	Manual shut-off valves	44
4.6	Thermal expansion valves (TXV).....	44
4.7	Electrically operated expansion valves	47
4.8	Pressure relief valves.....	48
4.9	Sight glass	49
4.10	Filters/driers	51
4.11	Service valves	52
4.12	Capillary hoses.....	55
4.13	Pressure switches	55
4.14	Summary of test results	56
	References.....	59
	Appendix 1: List of tested components.....	61
	Appendix 2: LFR measurements.....	71
A.1.	LFR measurement of Solenoid valve n°1:.....	71
A.2.	LFR measurement of Solenoid valve n°2.....	71
A.3.	LFR measurement of Solenoid valve n°3:.....	72
A.4.	LFR measurement of Solenoid valve n°4:.....	72
A.5.	LFR measurement of Flare fitting n°3.....	73
A.6.	LFR measurement of Flare fitting n°4.....	73
A.7.	LFR measurement of manual shut-off valve n°2	73
A.8.	LFR measurement of TXV n°1	74
A.9.	LFR measurement of TXV n°3	74
A.10.	LFR measurement of TXV n°4.....	74
A.11.	LFR measurement of electrically operated expansion valve n°1	75
A.12.	LFR measurement of electrically operated expansion valve n°2	75
A.13.	LFR measurement of service valve n°3.....	75
A.14.	LFR measurement of Service valve n°4	76
A.15.	LFR measurement of Pressure relief valve n°1.....	76
A.16.	LFR measurement of Pressure relief valve n°2.....	76
A.17.	LFR measurement of filters n°4:.....	77
A.18.	LFR measurement of sight glass n°3 (torques : 10, 15, 20 and 25Nm):	77
A.19.	LFR measurement of capillary hose	78
A.20.	LFR measurement of pressure switches n°1 and n°2.....	78

1 Background of the research program

Leakages of HFC and HCFC refrigerants have an adverse impact on climate change both directly because these refrigerants are very powerful greenhouse gases and also indirectly because leaking systems are less energy efficient.

The purpose of this research program is to develop a guideline to minimize refrigerant leaks by using high performance joints to ensure that designs and products are adequate to provide a truly tight system. The guideline will recommend a method of test capable to measure leak flow rate in the range of 1 g/yr, and will indicate the best in class technologies for reaching high level of leak tightness.

2 Literature review on Commercial Refrigeration equipment

2.1 Commercial refrigeration equipment

Commercial refrigeration aims at storing and displaying food and beverages at different levels of temperatures. The cooling capacities vary from some hundred watts to 1.5 MW. The refrigerant used depends on the temperature necessary to preserve the fresh food and beverages on one hand, and frozen food on the other hand. The UNEP TOC report [UNEP 2011] describes three different families of commercial refrigeration systems: stand-alone equipment, condensing units, and centralized systems. The refrigerant choice depends on the levels of conservation temperatures and the types of systems.

2.1.1 Stand-alone equipment

Stand-alone equipment is installed in all types of shops such as beverage vending machines, ice cream freezers, and stand-alone display cases. As indicated in Figure 2.1, all refrigeration components are integrated in the machine. Stand-alone units are hermetic (circuit is entirely brazed or welded as seen in Figure 2.2) charged with small refrigerant charges ranging from 0.2 kg to 1 kg.



Figure 2.1: An example of stand-alone.

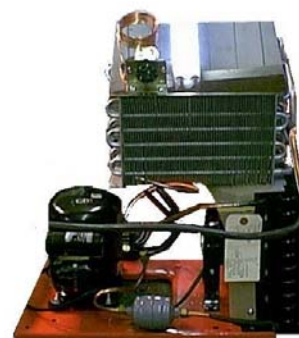


Figure 2.2: Refrigeration circuit.

Typical stand-alone equipments are vending machines, ice makers, ice cream freezers, water fountains, and plug-in display cases. For food kept at temperatures ranging from +1°C up to 10°C, HFC-134a is the dominant refrigerant.

2.1.2 Condensing units

Condensing units are usually installed in small shops where one or two compressors, one condenser and one receiver are assembled into a so-called “condensing unit” (see Figure 2.3), which is located out of the sales area. The cooling equipment includes one or more display cases (Figure 2.4) in the sales area or in a cold room for cold storage.



Figure 2.3: Condensing unit.



Figure 2.4: Display case.

Their cooling capacities vary from 5 to 20 kW mostly at medium temperature. Charges of these units are in the range of 1 to 5 kg. R-404A has been chosen to replace R-22 because of its high volumetric capacity. Nevertheless, in hot climate and for medium temperature applications, HFC-134a is used due to its higher energy performances at high ambient temperatures.

2.1.3 Supermarket refrigeration systems

Two options should be distinguished:

- When refrigerant evaporation occurs in the cooler, the system is called “**direct expansion**” system;
- When a low-temperature secondary heat transfer fluid (HTF) is cooled centrally and then circulated in a closed loop to the display cases, it is called “**indirect system**”. Figure 2.6 shows the principle of an indirect system with MPG (Mono-propylene-glycol) at the medium-temperature level and R-744 at the low-temperature level [CLODIC 2008].

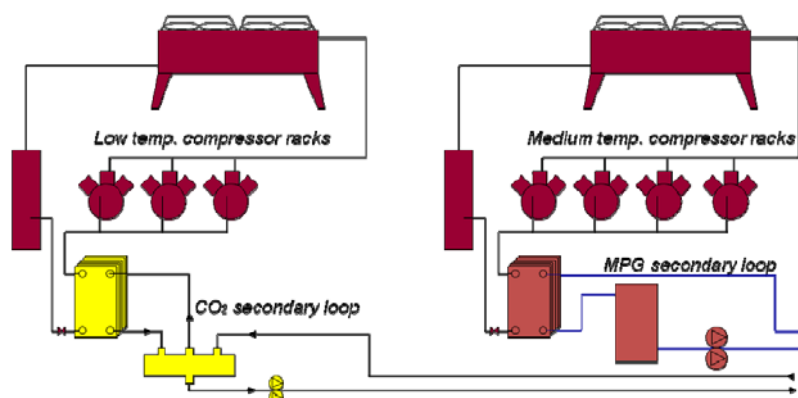


Figure 2.5: Indirect system with MPG(Mono-propylene-glycol) at the medium temperature level and R-744 at the low temperature level [CLODIC 2008].

Centralized systems (direct expansion) are the most commonly used. The system consists of racks of compressors located in a machinery room and air cooled condensers on the roof of the machinery room. This provides a cooling medium to display cases and cold storage rooms. Their sizes can vary from about 20 kW up to 1 MW of refrigeration capacity depending to the size of the supermarket. The refrigerant charge varies from 100 up to 2000 kg.



Figure 2.6: Compressor racks.

Parallel compressor racks include a number of mounted components that are all potential leak sources. Components including compressors, suction line, liquid and discharge manifolds, section control valves; 3-way valves, pressure controls, suction line filters, sight glasses, liquid receiver, oil separator, shut-off valves, etc.

According to [UNEP11] the refrigerant bank in 2006 was estimated at 340,000 metric tonnes and was distributed at follows:

- 7% in stand-alone equipments;
- 47% in condensing units, and
- 46% in centralized systems.

2.2 Leakage assessment based on literature

On a global basis, commercial refrigerant is the refrigeration sub-sector with the largest refrigerant emissions calculated in CO₂ equivalent. They represent about 40% of the total annual refrigerant emissions. Annual leakage rates higher than 30% of the system refrigerant charge have been found when performing top-down estimation [CLODIC 1998].

Table 2.1 summarizes the results of different studies for U.K. in the commercial refrigeration sector. Data show the highest leakage occurs in centralized systems representing about 10 to 20% refrigerant loss of the initial charge.

Table 2.1: Annual refrigerant leakage rates for UK [COWAN 2010].

	ETSU (1997)	Johnson (1998)	March (1999)	Haydock et al (2003)
Integral cabinets	2.5%	9 to 23%	1%	3 to 5%
Condensing units	15%		10 to 20%	8 to 15%
Centralized supermarket systems	8%		10 to 25%	10 to -20%

Based on [BIVENS 2004], data from supermarket organizations across the United States summarize a total of 349 stores reported average refrigerant loss rates in the range of 8 to 15% per year in 1993 and 1994. Report [TROY 1997] showed refrigerant leakage losses of 18% and 22% of the system inventory. Figure 2.7 presents the leakage loss by charge size. It can be seen that from 2000 to 2001, except for extra small units, the refrigerant charge varies from 10 to 23%.

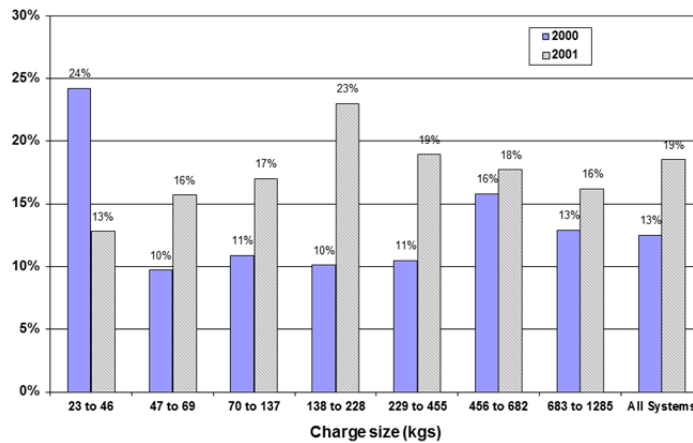


Figure 2.7: Annual refrigerant emissions rates (California South Coast Air Quality Management District).

Leaks from direct emissions result from vibration and thermal expansion of numerous pipes, threaded joints, fittings, and valves. Ruptures can result in huge refrigerant losses. High indirect emissions come from energy inefficient system components, inappropriate designs, or lack of heat recovery in some systems, etc. [IEA 2003] shows the estimated TEWI (Total equivalent warming impact) of refrigeration systems in Washington, DC. As given in Table 2.2, the distributed and secondary loop systems both showed significant reduction in TEWI, compared to multiplex systems.

Table 2-2: TEWI for commercial refrigeration.

System	Condensing	Charge (lb)	Refrigerant	Leak (%)	Annual Energy (kWh)	TEWI (million kg of CO ₂)		
						Direct	Indirect	Total
Multiplex	Air-Cooled	3,000	R404A/	30	976,800	13.62	9.52	23.15
	Evaporative	3,000	R-22	30	896,400	13.62	8.74	22.36
Low-Charge Multiplex	Air-Cooled	2,000	R404A/	15	935,200	4.54	9.12	13.66
	Evaporative	2,000	R-22	15	863,600	4.54	8.42	12.96
Distributed	Air-Cooled	1,500	R404A	10	860,500	3.33	8.38	11.71
	Water-Cooled, Evaporative	900	R404A	5	866,100	1.00	8.44	9.44
Secondary Loop	Evaporative	500	R507	10	875,200	1.13	8.54	9.67
Secondary Loop	Water-Cooled, Evaporative	200	R507	5	959,700	0.23	9.36	9.58
Advanced Self-Contained	Water-Cooled, Evaporative	100	R404A	1	1,048,300	0.02	10.22	10.24

Results for site in Washington, DC – 15 year service life.
 Conversion factor = 0.65 kg CO₂/kWh.
 Multiplex – 33.3% R404A (low temperature), GWP = 3260; 66.7% R22 (medium temperature), GWP = 1700.
 Distributed and Advanced Self-Contained – 100% R404A, GWP = 3260.
 Secondary Loop – 100% R507, GWP = 3300.

Figure 2.8 summarizes the locations of refrigerant losses in 62 commercial refrigeration systems in 1999 [BIRNDT 2000]. It can be seen that the main leak contributor is the flare joint 22%, followed by the sight glass 16%. Service valves, flanges, screw joints, etc. are also leakage contributors.

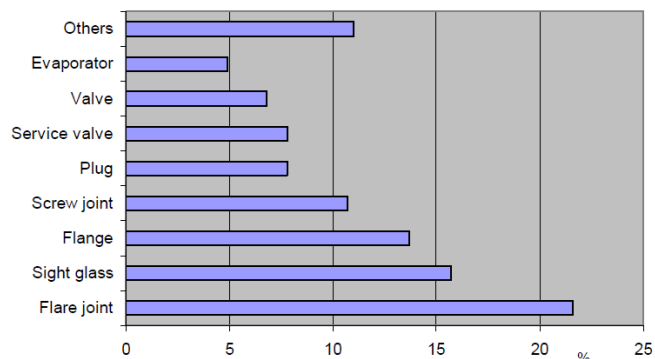


Figure 2.8: Locations of refrigerant losses in 62 commercial refrigeration systems in Hesse and Saxony in 1999 [BIRNDT 2000].

Preventing the system from leaking depends on the good design, service, and maintenance. In order to reduce refrigerant loss, it is essential to understand where and why leakage occurs. Next section focuses on the description of the commonly used components and their joining techniques allowing the understanding of those joining techniques.

Other studies [CLODIC 1998] and field surveys [RALEY's 2005] have shown that a limited number of leak prone components are the source of overall refrigerant emissions. In summary, a large number of components are leak tight and a few are not and generate large emissions. One of the objectives of this report is to identify which component designs imply default of leak tightness and also which emissions are related to neglectful mounting.

2.3 Description of commonly used components and identification of their joining techniques

Joining techniques include:

- Welding and brazing that require qualified personnel, proper brazing or welding equipment, and proper choice of filler composition. Moreover to avoid oxide formation, a nitrogen flow inside copper tubes during brazing avoids oxide formation.
- Mechanical assembly, comprising many possible arrangements and include elastomer materials inserted between two metallic surfaces. The sealing material presents contradictory properties: nearly incompressible but with an elasticity (or viscoelasticity) enabling deformation leading to “fill the gap” of clearances between the two solid surfaces. The viscoelasticity implies a low Young's modulus and high failure strain NBR. Young's modulus varies between 2 and 5 MPa and the one of PTFE is 500 MPa; those most used materials for seals are so quite different in terms of deformations and thus capability of sealing depending on the torque delivered to the mechanical joint.
- In terms of seal designs the shapes are of two main types: torus (o-ring), flat ring, and cones
 - O-ring seals present one of the most reliable mechanical assembly providing the definition of clearances between the O-ring and its groove.
 - Flat seals are more sensitive to the torque compared to O-rings, especially those made with PTFE (Teflon) that require proper torque, as shown in test results.
 - Conic seals are mostly used for flare joints with or without copper gaskets. To be noted that the Young's modulus of copper is of 117 GPa, a factor 1,000 compared to PTFE and 100,000 compared to NBR; consequently, the torque to reach the same level of deformation is much different.

The report presents the number of possible arrangements of those seals for valves of different designs, electro-valves, valve stems, pressure switches, sight glasses, safety valves, and filters. All those joining techniques have in common the integration of either metallic or rubber or elastomeric seals. So the study is evaluating the efficiency of the most used sealing techniques.

Based on commercial refrigeration detailed in Section 2, main refrigeration components and their joining techniques are described in this section. All cutaways have been done by EReIE in order to analyze the joining technique.

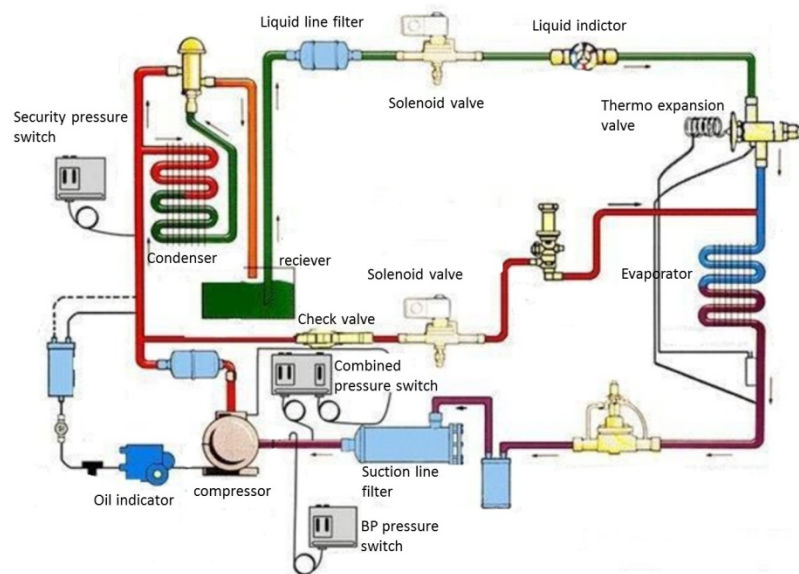


Figure 2.9: A typical commercial refrigeration circuit.

2.3.1 Thermo expansion valves

A thermostatic expansion valve ensures a constant superheat at the evaporator outlet. The valve controls the liquid refrigerant so that the evaporator coils can maintain the correct amount of refrigerant at all times. Figure 2.10 shows the valve cutaway.

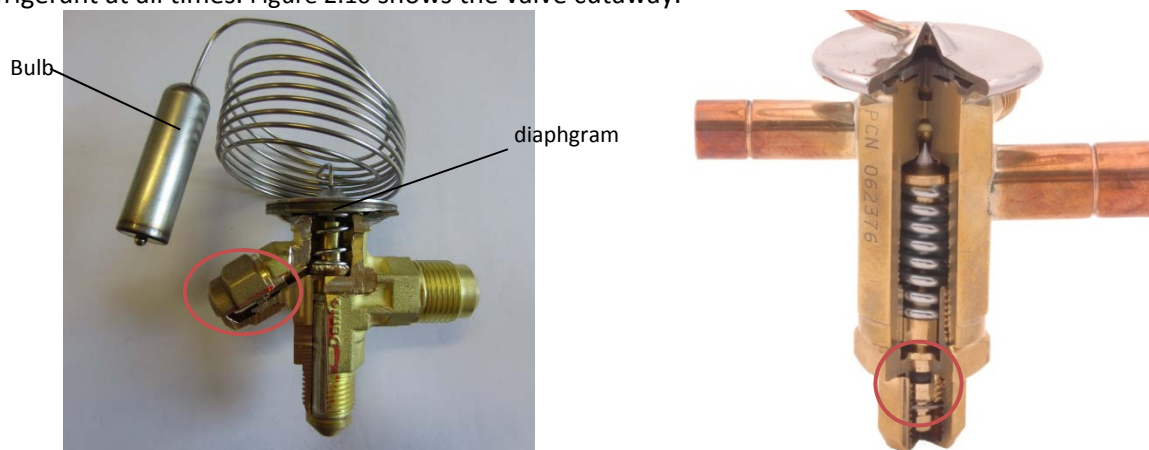


Figure 2.10: Thermo expansion valves.

The bulb, attached to the evaporator outlet, senses the superheat at the section line and adjusts the flow of refrigerant into the evaporator. When the superheat increases, the temperature and the pressure in the remote bulb increase. Pressure, applying to the top of the diaphragm, forces it down along with pin, which opens the valve passage, admitting more liquid refrigerant to pass to absorb heat from the evaporator. Second, it applies higher pressure to the bottom of the diaphragm, forcing it upward, tending to close the valve. Third, it reduces the degree of superheat by forcing more refrigerant through the suction line. O-ring seal is used for sealing the regulator of the valve initial position.

2.3.2 Manual service valves

Using the service valve on both suction and discharge lines of a compressor allows the isolation of the compressor from the refrigeration system and provides quick access to low or high-side pressure.

Moreover, using this valve, refrigerant from the compressor can be recovered without requiring recovery of the complete system charge.

Compressor 3-way service valve

Compressor service valves are usually located on the suction and liquid lines allowing the measurement of the low or high-side refrigerant pressure. By definition, the service valve is equipped with three valves. Figure 2.11 shows the detailed structure of a service valve. It can be seen that the service valve is equipped with three connections that are the compressor connection, the refrigerant line connection, and the service port. The compressor side connection is made of a “rotolock” valve, as shown in Figure 2.11. The valve is a specific refrigeration valve with a Teflon ring seated against a machined surface enclosed by a threaded fitting. This valve is easily installed and removed rapidly.

Three positions of the service valve correspond to different operations:

- **Back seated:** the stem is turned all the way counterclockwise. The service port is closed but the compressor port is open to the refrigerant line port.
- **Front seated:** the stem is turned all the way in clockwise. The line port is closed but the compressor port is open to the service port.
- **Middle position:** when the stem is turned $\frac{1}{2}$ turn off of a fully seated position, all the three ports communicate. The valve is just off the seat, creating a small opening.

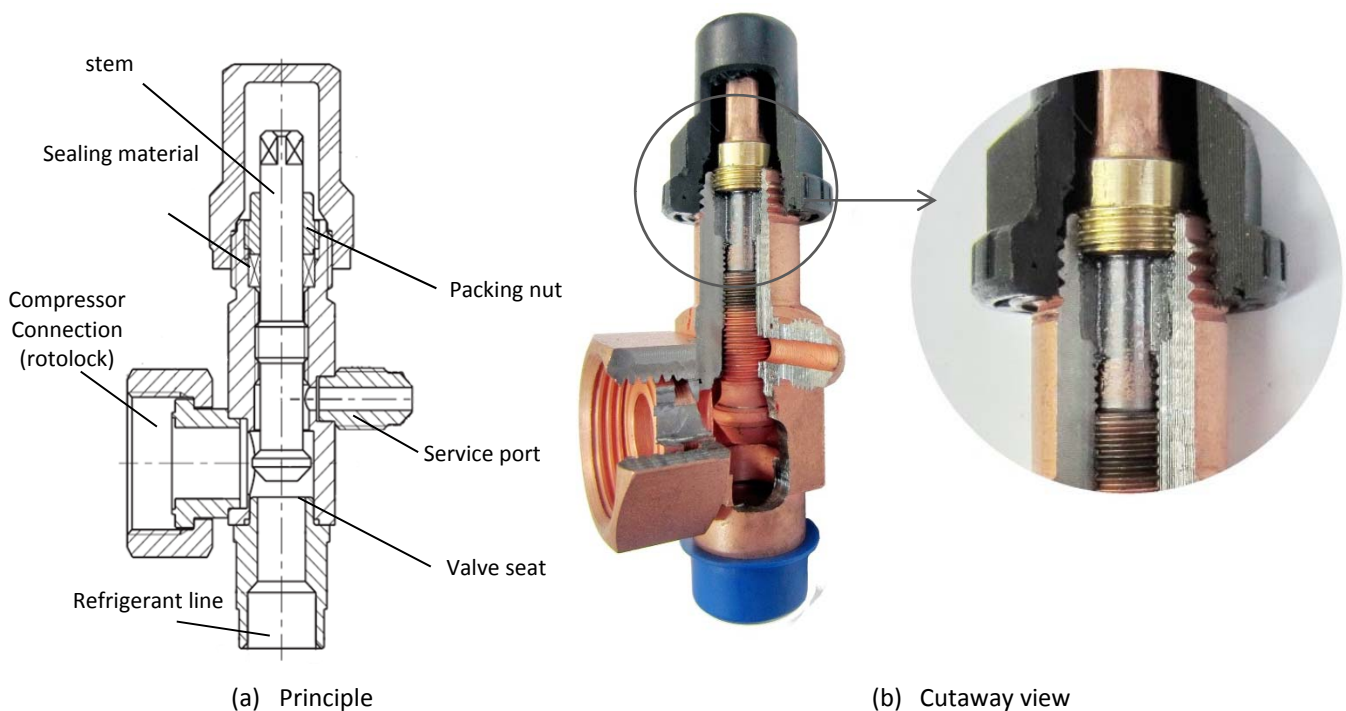


Figure 2.11: Compressor 3-way service valve.

Apart from three connections, which are possible leakage sources, the leak tightness between the stem and the valve body is made by compression of the carbon seal by the packing nut (Figure 2.11 (b)). Attention should be paid to the degradation of the leak tightness of this joining technique. Tests will be carried out first on a new factory-made valve and then by tests after a series of handlings. The first test list agreed with AHRTI is presented in Appendix 1. Most of those components have been tested. Some new ones have been chosen and tests are described in the report. All tests and components are summarized in Table 4.25.

Angle type service valve

This type of service valves are used on most of semi-hermetic compressors or commonly on the liquid receiver.

As illustrated in Figure 2.12, the valve stem moves back and forth to open and close the valve from its seat. The stem passes through a nut on the outside of the valve. 2 rubber (CR) gaskets and 2 gaskets (Aramidic-fibers) are compressed when the nut is threaded down into the valve seat and prevent the valve from leaking. Inlet and outlet of the valve is thread and flare connections.

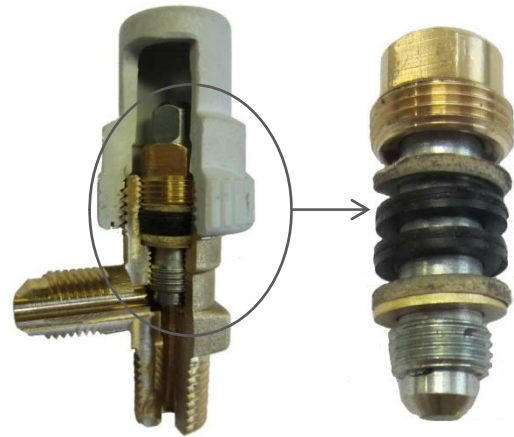
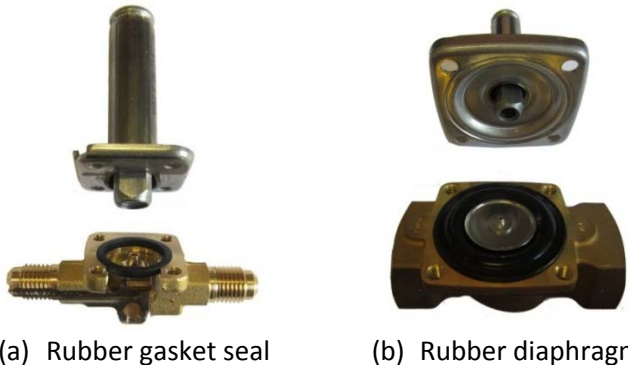


Figure 2.12: Angle-type service valve.

Comparison between different joining techniques of service valve should be done to find out the best leak-free sealing method.

2.3.3 Solenoid valve

The electrical driven solenoid valve is generally used to isolate the circuit. Generally the valve bodies and the electrical coils are two separated parts.

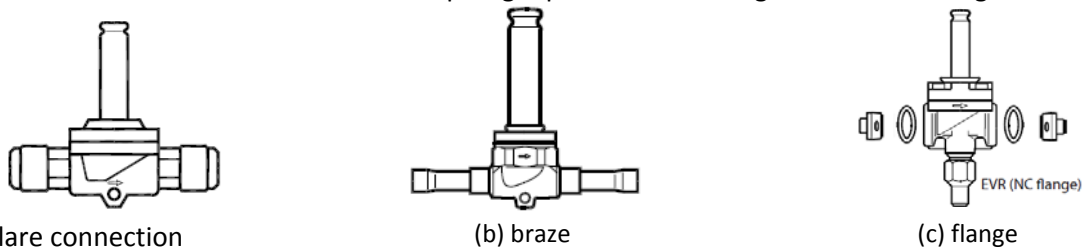


(a) Rubber gasket seal (b) Rubber diaphragm

Figure 2.13: Joining techniques of solenoid valves.

Figure 3.5 shows the joining techniques of two solenoid valves without electrical coils. The valve body is made of brass; the armature tube and the cover are made of stainless steel. Sealing part in Figure 2.13(a) is a gasket rubber. 4 screws fix the plate of the armature to the valve body, compressing the rubber gasket to ensure the valve leak tightness.

As shown in Figure 2.13(b), the valve is operated by a floating diaphragm. The orifice is located in the center of the diaphragm, and the Teflon pilot valve plate is fitted directly to the armature. The rubber border of the diaphragm prevents the refrigerant from leaking outside.



• (a) flare connection

(b) braze

(c) flange

Figure 2.14: Different valve connections (by courtesy of Danfoss).

2.3.4 Manual shut-off valve

The manual valve is fitted with a diaphragm made of stainless steel. As shown in Figure 2.15, the valve body, cover, and spindle are made of brass. The tension in the diaphragm lifts the valve plate from the seat when the valve is open.

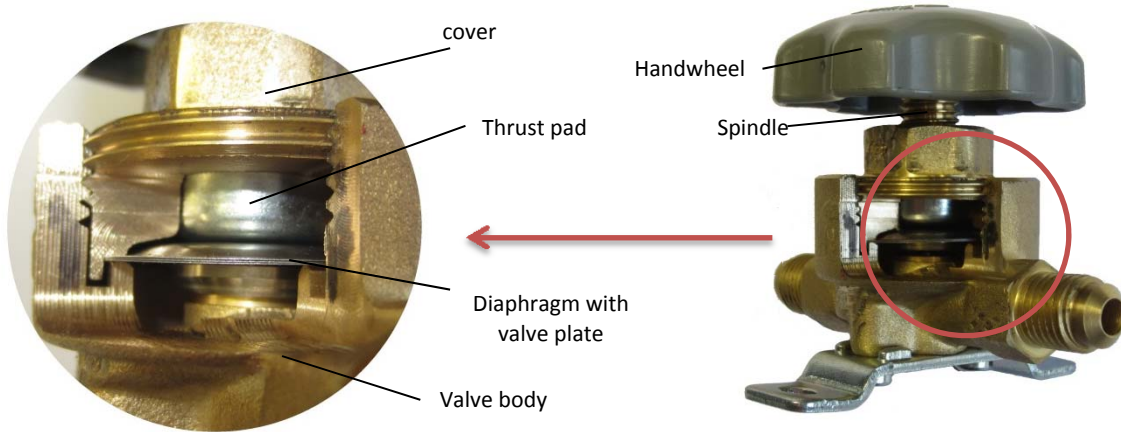


Figure 2.15: Cutaway view of a shut-off valve.

The edge of the diaphragm is used as seal. Compression between the cover and the valve body prevents the valve from leaking.

2.3.5 Ball valves

Ball valves are used in liquid lines in refrigeration circuit. The ball valves let maximum flow go in open position (1/4 turn) and isolate the passage when closed (1/4 turn). As shown in Figure 2.16, the valve is equipped with an access port by Schrader connections.

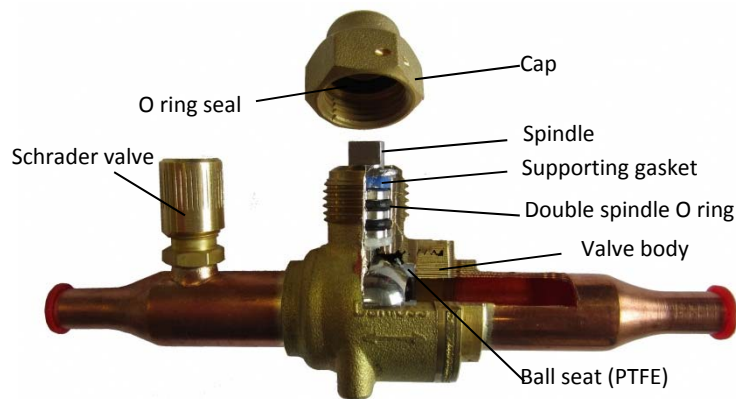


Figure 2.16: Cut away of a ball valve.

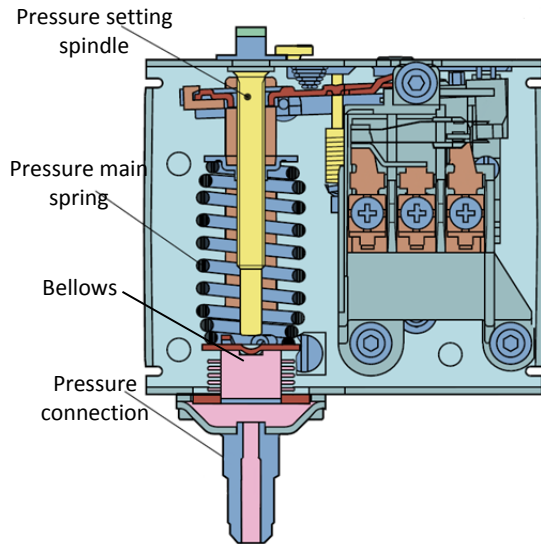
It can be seen from Figure 2.16 that the valve body is welded. The valve ball and the spindle are made of stainless steel. Besides the welded valve body and the ball seat/seal (PTFE), the leak tightness of the valves is ensured by the double O-ring seal made of rubber. Moreover, the cap is equipped with an O-ring seal. Leakage will be measured not only on new valve but also after aging by handling.

2.3.6 Pressure switches

Pressure switches are used in refrigeration to protect against excessively low suction pressure or excessively high discharge pressure.

- Single pressure switches

Pressure control switches are mainly used to control the compressor start and stop. The pressure acts on the bellows of the pressure connection that produces movement of a mechanism operating electrical contacts.



(a) Principle (by the courtesy of Danfoss)



(b) Expanded view

Figure 2.17: Single pressure switches.

Figure 2.17(a) illustrates the principle of the pressure switch. A pressure rise closes the switch contacts and there by completes the circuit of the controller, which starts the compressor automatically. As the operation of the compressor gradually decreases the suction pressure, the movement of the switch linkage reverses until the contacts are separated at a pre-determined low-suction pressure, thus breaking the controller circuit and stopping the compressor.

As shown in the expanded view of the connection, the pressure is contained in the bellows made of copper that is “crimped and brazed” to the flare fittings. Bellows move only when the set point valve is reached and there is no relative movement of two separated parts. Without exceptional bellow rupture, leakage comes only from the flare connection.

- Combined pressure switches

The combined pressure switches control both the high and low pressure levels of the refrigeration circuit. The joining technique is the same as the single one, the tube is connected by either flare connection or capillary copper tubes with female flare fittings at the ends.

With vibration, the brass can be damaged or tubes rub against a surface leading to cracks causing leakage.



(a) Flare connections



(b) Capillary tube with female flare ends

Figure 2.18: Pressure-switch connections.

2.3.7 Pressure relief valve

The pressure relief valve is an important safety device controlling the maximum pressure allowed to build up inside the refrigeration circuit. The high-pressure circuit is usually equipped with a relief valve to prevent extreme high pressure and protect the components.

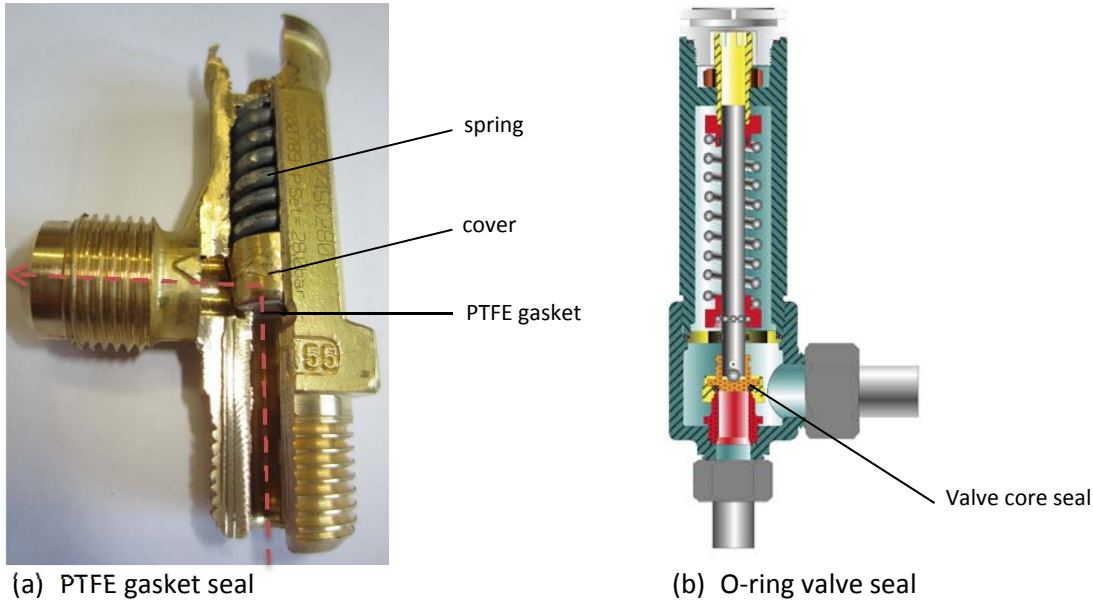


Figure 2.19: Pressure relief valves.

The spindle is held in contact with the seat by a spring. The spring is compressed by a screw on the top of the valve body. High pressure lifts the seal and spindle from the seat and allows the refrigerant to pass through. One of the main external leakages is associated to the fact that after an opening the spindle is not coming back to its initial stage and so a continuous flow is occurring.

Fusible plugs (see Figure 2.20) are used often on liquid receiver. Large temperature and pressure variations weaken the bond between the brazed core and the plug and causes leakage.



Figure 2.20: Fusible plugs.

2.3.8 Schrader valve

The Schrader valve is a spring-loaded valve with a core threading down in to it. When a hose with a core depressor is connected to the Schrader valve, the core is pushed in and the refrigerant is allowed to pass through the core. As illustrated in Figure 2.21, the fitting body is made of brass. The three main parts for sealing are as:

- Rubber for the cap O-ring seal;
- Rubber/PTFE for the outlet seal;
- Rubber for the seat gasket.

Moreover, the cap is equipped with an O-ring to prevent leakage outside, which is why the Schrader valve should always have its leak-proof cap in place when not in use.

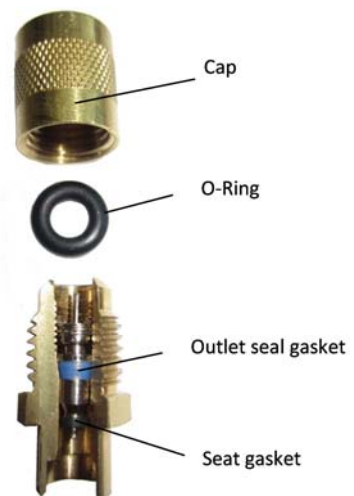


Figure 2.21: Cutaway view of the sealing techniques of a Schrader valve.

Leak causes should be different for the valve: the rubber seals may deteriorate or the valve gets stuck over the time; the core has not been correctly tightened; the valve core left in the valve by mistake could be damaged during brazing, etc.

2.3.9 Sight glasses

Liquid indicators (sight glasses) are specific fittings provided with a gasket around the glass with a single or a double port. Sight glasses are located on the liquid line upstream the TXV.

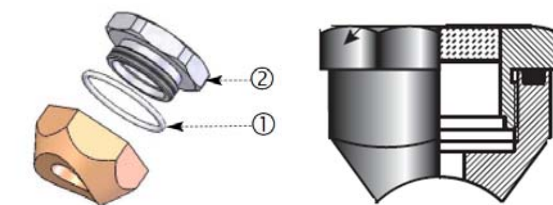
As shown in Figure 2.22, connections are equipped with built-in sight-flow indicator:

- Brazed ends
- External/external flared ends
- External/internal flared ends

As illustrated in Figure 2.23(a), two parts of the indicator are sealed by a Teflon gasket; the end is brazed on the liquid line, and provided with or without seal caps for protection when not in use.



Figure 2.22: Different liquid indicators.



(a) Gasket sealed



(b) Hermetically sealed sight glass

Figure 2.23: Cutaway view of liquid indicator.

2.3.10 Filters

Filter driers are located on the liquid line (liquid line filter) and suction line (suction line filter) for the purpose to remove moisture from the refrigerant by adsorbing and retaining it deep within the desiccant granules; to filter out residual braze particles, carbon, dirt or any other foreign matter; to adsorb the hydrochloric, hydrofluoric, and various organic acids allowing to clean up the oil and assure the performance of the system.



Figure 2.24: One body filter.



Figure 2.25: Replaceable suction line filter (by courtesy of Sporlan).



Figure 2.26: Replaceable filter and its gasket for sealing.

Filters can be one body (Figure 2.24) or replaceable (Figure 2.25), which is in the form of flanged shell holding replaceable pleated filter elements. Except its inlet and outlet connections, one body filter can be considered as leak free. This is not the case for replaceable filter. As shown in Figure 2.26, gasket made of aramidic-fibers ensures the filter leak tightness. Figure 2.27 shows another type of replaceable filter. The filter elements are assembled with a screwed end with its PTFE gasket.



Figure 2.27: Replaceable filter.

Because of the present joints, inadequate or uneven tightening of the flange will often lead to leakage.

2.3.11 Flare fittings

As observed throughout the report, flare fittings are widely used to provide a mechanical connection between copper tubing and fittings. As shown in Figure 2.28, flare fittings are divided into two main parts: male and female parts. The type of fittings having visible threads on the outside is a male one and the opposite part is the female part, which has threads on the inside.

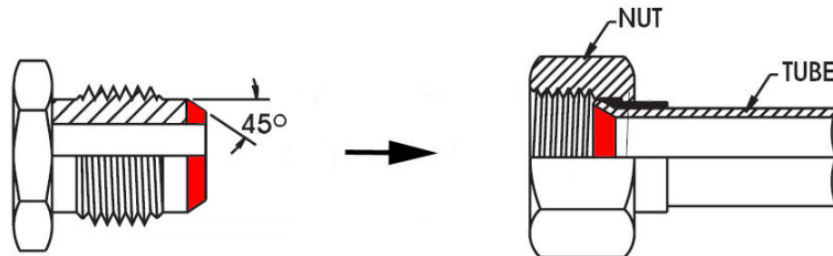


Figure 2.28: Flare connections.

The seal is purely metal to metal seal and is the result of two sloped surfaces coming together. Figure 2.29 shows flare connections for different usages.

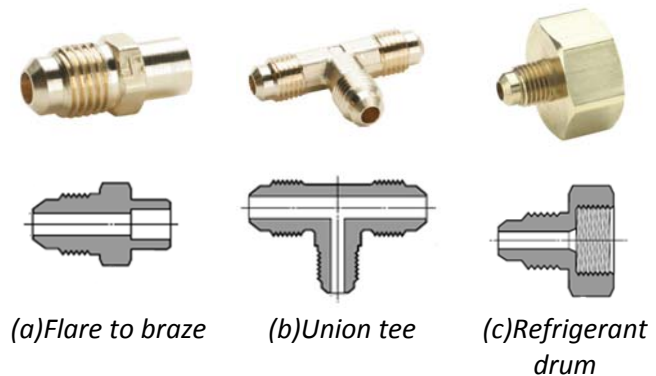


Figure 2.29: Flare connections.

The tubing flared end is made with special tools. The tubing end should be properly cut and reamed before attempting to make flares. Rough edges will interface with the smooth metal-to-metal contact and cause leakage. One can forget to clean the surfaces or over-tighten the fittings. Both can cause the flare fittings to leak as well. Figure 2.30 shows a leakage detected at flare fittings. Leaks can occur from threaded and flared fittings either when they are not tightened sufficiently or when they are over-tightened and crack. A case study, performed by Hill Phoenix Refrigeration, indicates that leak rates at flare fittings detected within the factory-controlled environment exceeded all other leaks on the rack systems.



Figure 2.30: Leaks at flare fittings.

It should be pointed out that flare fittings realized in factories or in the field in difficult positions do not have the same leak tightness level. Additional constraints due to assembly will amplify this effect.

- Flare fittings with copper gasket

High pressure variations and duty cycle can lead to the weakness of metal to metal flare sealing faces, making leak prone assembly. To enhance flare fitting leak tightness, copper gaskets are largely used (see Figure 2.31). Due to the conical design of the mating surface, different types of metal conical seals exist: copper flare bonnet, copper flare gaskets or gasket with Long Tan (ENALT design) [INT 08]. It is said that they provide more clearance and flexibility for tightening flare nuts. Leak tests should be done in order to verify how leak tightness is improved by such gaskets sealing techniques.



Copper flare gaskets



(a) Gasket with long tan
Figure 2.31: Flare fitting gaskets.



(b) Copper flare bonnet

- Double flares

The double flare is formed by bending the end of the copper tube and folding it together. Figure 2.32 shows an illustration of double flared tubing. It is smoother and more concentric than the single flare and it is also more resistant to the torque shearing effect.

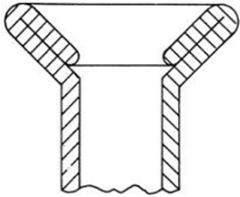


Figure 2.32: Double-flared tube ends.

A double flare is necessary to prevent cutting off the flare and failure of the tube assembly under operating pressures. The double flare is non-commonly used. No data prove that the leak tightness of double flare is better than the single one. Tests can be performed to assess if the double flare design improves leak tightness of flare fittings.

- Flare fittings with seal

In 2000, Flaretite released a new sealing: the Flaretite Seal designed to eliminate leaking flared type fitting joints. The seal is a stainless steel stamping, designed with multiple concentric rings. The entire seal is impregnated with a baked-on Loctite coating.

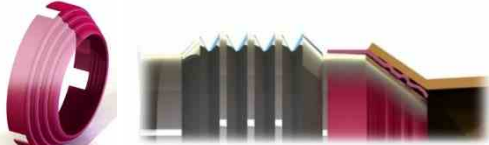


Figure 2.33: Flaretite seal.

According to the supplier, when inserted into a flared fitting joint, the concentric rings form multiple seals down the face of the flare and the Locktite coating fills minor imperfections. The sealing rings prevent environmental contamination and aggressive cleaning solvents from attacking the seal face. Tests should be done to compare the leak tightness of single and double-flares with a multi-ring seal coated with an industrial suitable sealant.

2.3.12 Heat exchangers (evaporator and condenser)

Heat exchangers are copper tube made and brazed coils. Copper tubes are connected together by brazing the U shape tube at the end as shown in Figure 2.34. Leak occurs at the U tubes at the end of the coil. Over time and under vibration, leaks will occur. Corrosion on the condenser side because outdoor climate or on the evaporator side in contact with food acids may corrode and develop pinhole leaks. Brazed joint will be described in detail in the next section.



Figure 2.34: Brazed joint of coil

2.3.13 Brazed joint

Copper tubes are used in refrigeration circuits to joint different components due to their chemical compatibility with refrigerants. Different copper parts are joined by brazing and brazing with capillary brazed joint fittings. Good brazing joints should be strong, withstand vibration, temperature, and thermal cycling stress.

Socket joints are commonly found for brazed joint because two parts are self-aligning during assembling. As shown in Figure 2.35, male part is inserted into the socket and the overlap length allowing braze to fill in and forming the bonding area. The key variables are as follows.

- **Filler metal:** copper-phosphorus is recommended for making not detachable joint
- **Applied Heat:** Most brazing for refrigeration are done at temperatures ranging from 600°C to 815°C.
- **The amount of filler:** when the joint is complete, continuous filler should be visible completely around the joint.

According to the American Welding Society, the strength of the brazed joint will meet or exceed that of the tube and fitting being joined when the depth of filler metal penetration is a minimum of 3 times the thickness of the thinner tube. The strength of a brazed copper tube joint does not vary much with the different filler metals but depends on maintaining the proper clearance between the outside of the tube and the fitting cup.

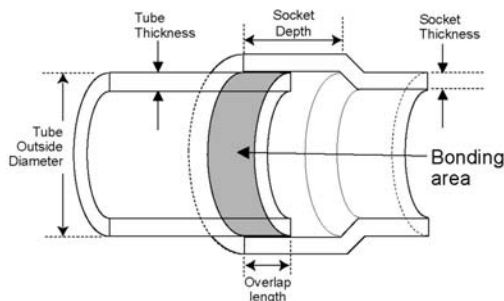


Figure 2.35: Socket type brazing joint.



Figure 2.36: Copper fittings.

Figure 2.36 shows a series of copper fittings such as 90° bend, 45°, 90°, and 180° elbows, tees, line connector, etc. which are commonly used on pipework joints of refrigeration systems.

Oxide scale on the inside of tube can cause problems when refrigerant and lubricant is circulated in the system (leading to sludge formation). Nitrogen introduction as protective gas at low flow rate inside the pipe assembly during brazing process is a common method to avoid oxidation. Figure 2.37 shows clearly the formation of oxide on the inner side of the brazing joints.

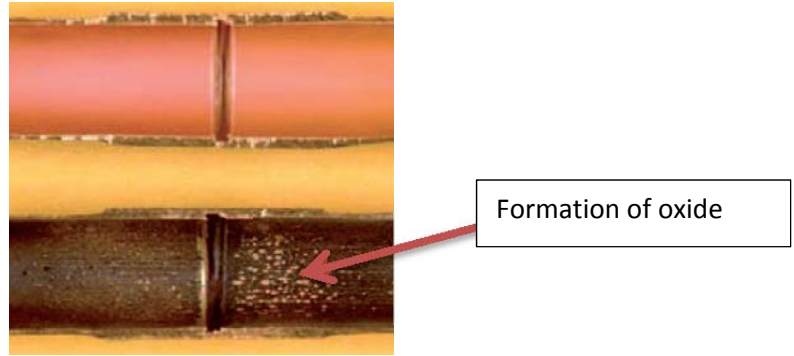


Figure 2.37: Brazing joints with/without nitrogen purge.

The good practice for joining processes (copper to copper and brass to copper) is summarized in Table 2.3.

Table 2.3: Good practice for copper brazing in refrigeration circuit

Step	Copper to copper	Brass to copper
Cutting ends	The tube should be cut clearly without deformation so that it can seat properly in the socket;	
Reaming	Small burrs / rough edges should be removed to avoid local turbulence and increased velocities in the tube.	
Cleaning	Tube end should be clean by removing the oxides and surface soil to guarantee that the filler material flows properly inside the gap. The internal surface of the fittings should be cleaned as well by using a brush. Oxides, surface soil, and oil can interfere with the strength of the joint and this may result in the joints failure.	
Assembly	Both tube and fitting assembled together, right joint depth should be guarantee	
Fluxing:	(No flux is needed as the vaporized phosphorus will remove the copper oxide film.) Flux used for brazing may also contaminate the environment inside tubing and must be removed after the brazing process.	When brazing brass fitting to copper tube, a water soluble flux should be used
Nitrogen introduction	Introduce slow flow of dry Nitrogen for purging and preventing oxide formation on the inner surface.	
Heating	Heat evenly to the area on both tubing and fitting interface and apply heat evenly until brazing temperature is reached.	The same as for copper to copper, only more heat should be concentrated on the brass fitting to bring it to temperature.
Applying filler metal	When well heated, the melted filler metal will be drawn into the joint by capillary action. Special copper tube fittings designed for refrigeration service should be used since they are produced with close tolerances to ensure tight capillary joints in the brazing process. Using a silver/phosphorus/copper alloy with between 5% and 15% silver, braze refrigerant line with nitrogen flowing through the line to eliminate carbon deposit buildup on the inside of the joints, which could contaminate the refrigerant.	
Cooling and cleaning	After brazing, joints are left to cool in the air, stop the purge of Nitrogen	

Leaks can result from poor brazing joints such as:

- Improper join preparation prior to brazing
 - Lack of proper support or hanging during brazing
 - Improper heat distribution through the entire joining process
 - Improper application of brazing filler metal to the joint
 - Horizontal brazing joint results in inadequate amount of filler metal applied to the joint
 - Using the wrong brazing alloy

Tests will be performed by simulating different conditions to investigate the effects.

2.4 Leak detection method review for air-conditioning and refrigeration systems

2.4.1 Leak detection methods

This section makes an overview of the leak detection methods and helps to choose the most appropriate ones. Two types of detection should be distinguished here:

- Leakage location: leak sites are located;
- Leakage quantification: leak flow rate of a given component is precisely measured.

2.4.1.1 Leakage location

A variety of methods exists to locate leaks for air conditioning and refrigeration systems. The most commonly employed techniques are described here below [MALEK 1995], [INT03].

Immersion method

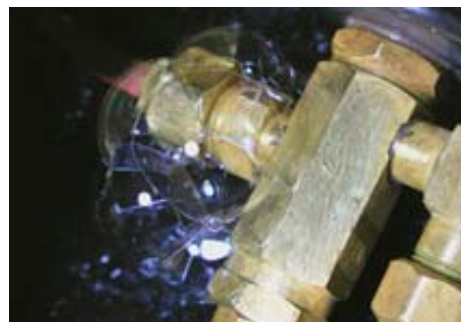
The water immersion is a traditional and commonly used leak detection method. During the testing process, the area of the suspected leaks is pressurized with air or nitrogen and immersed into a water tank. The formation of bubbles in the water indicates a leak. This method is reliable and easy for detecting large leaks. However, relatively small leaks are difficult to detect. According to literature [INT01], the sensitivity of this method is considered as 10^{-4} Pa.m³/s. The disadvantages of this method are: the component contacting with water needs to be dried after test, complexity of handling large parts during immersion and the level of leak flow rates are **higher than 10 to 40 g/year**.

Soap bubble method

Instead of immersing test component in water, a pressurized concentrated soap solution is sprayed at suspected leak locations. The escaping gas causes soap bubbles to develop. Figure 2.38 (a) and (b) show examples of micro leak and large leak detected by soap bubble spray [INT06]. This method is simple, rapid and not expensive. Leaks can be easily pinpointed using this method.



(a) Micro leak



(b) Large leak

Figure 2.38: Leak detected by soap bubble.

The sensitivity depends on the internal pressure. According to [CLODIC 2000], it can detect leaks **between 10 and 30 g/yr** depending on the internal pressure, which is out of the scope of the present study. This method is usually used to verify the leak tightness of brazing joints before charge. However, for small leaks, soap solution may dry out before bubbles develop, many leaks may not be found. These factors make this method adapted to large leaks (> 10 g/yr) only.

Fluorescent Leak Detection

The method requires adding fluorescent dye to the refrigeration system. The dye mixes with the lubricant and circulates with the refrigerant through all parts of the system. The lubricant escapes out, so does the dye. It remains at leak location and can be detected. As illustrated in Figure 2.39 (b), when the system is scanned by an ultraviolet or blue light torche, the dye shows bright yellow green color spots that can be easily identified.



(a) Injection of fluorescent dye



(b) Leak detection by UV torch

Figure 2.39: Fluorescent leak detection method.

The fluorescent dye method of leak detection is safe, inexpensive, and easy to use. It allows the detection of leaks on several sites during a single inspection. The compatibility of the dye with the system (fluid and the lubricant) should be verified to avoid premature failure of the components. Moreover, when the system is equipped with oil separation devices, the effectiveness of this method will be reduced. If the test duration is longer than 10 hours and internal pressure in the range of 500 kPa, leaks of **about 5 to 10 g/yr** can be detected.

Sniffing method by portable electronic leak detector

Two basic technologies are used by portable electronic leak detector: Corona discharge detector and heated-diode leak detector.

Corona discharge detector works by creating a high-voltage corona in the sensing tip. Gas sample entering the sensor reduces the corona emission that changes in current drop. The greater the current drop, the higher the concentrated of gas. Figure 2.40 presents a Corona discharge detector. According to constructor, it can detect a leak **less than 14 g/yr**.



Figure 2.40: Corona discharge detector (Robinair).

Heated-diode leak detector utilizes positive ion emissions into ambient air from a red hot wire. The system consists of a ceramic element that heats refrigerant gas and breaks apart the molecules, leaving positively charged chlorine or fluorine ions that are attracted to a negatively charged center collection wire. The flow of chlorine or fluorine ions to the center collection wire creates a small

current. As the refrigerant concentration between the electrodes increases, the current increases to a level that sets off an audiovisual alarm.

A heated-diode leak detector (*Inficon*) and its sensor are presented Figure 2.41. It should be pointed out that the sensor can be damaged if it detects a high concentration of refrigerant gas and the component is scarified over time. Depending on detectors, detection sensitivity can reach **2 g/yr**.

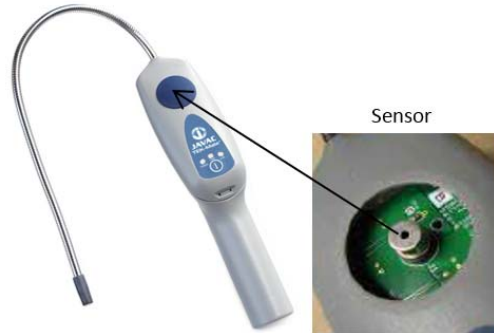


Figure 2.41: Heated-diode leak detector (Inficon).

Sniffing detection method is high operator dependent. Careful attention should be paid when scanning the component for leaks. A calibrated leak should be used during leakage detection to verify the detector. According to [Morgado 2008], the detection is more efficient if the detector nose is directed to the leakage direction.

As illustrated in Figure 2.42, (b) is much better than (a). Moreover, the leak detector nose should not be farther than 2 mm of the leakage location and the moving speed should be in the range of 2 mm/s.



(a)Scan from the top

(b)Scan from the bottom

Figure 2.42: Direction of detector scan.

Envelopment method

The method is shown in Figure 2.43. The suspected component is enveloped by a vinyl sheet closed by adhesive tape [CLODIC 1998]. The escaped gas accumulates in the envelop; then it can be easily detected by an electronic detector. Because the vinyl sheet adapts to different shapes, this method can be used for various components. The accumulating time can be long depending on the leakage level.



Figure 2.43: Example of a valve wrapped in a vinyl sheet [CLODIC 1998].

This method has been developed to quantify the leakage. Once the accumulation volume is well known and the exact quantity accumulated inside can be precisely measured, the leak flow rate can be calculated. Sensitivity is lower than 1 g/yr for a waiting time of 30 minutes.

Table 2.4 presents the comparison of measurement methods described previously.

Table 2.4: Comparison of measurement methods

Method	R-134a MFR* (g/yr)	Localization method	Global measurement
Immersion	10 - 30	X	
Soap bubble	10 - 40	X	
Fluorescent leak detection	5 - 10	X	
Sniffing method by portable electronic leak detector	1 - 2	X	X
Envelopment	0.1 - 1		X

*MFR: minimum leak rate level that can be detected

2.4.1.2 Leakage quantification by tracer gas leak testing

Quantification of leakage defines the overall leak flow rate of a given component instead of finding out its position. Tracer gas testing measures the flow rate of a tracer gas through a component under test. As shown in Figure 2.44 [INT02], the tested component is charged with tracer gas and installed in an enclosed accumulation chamber.

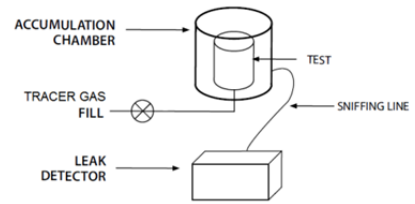


Figure 2.44: Accumulation method.

The leak is tested inside-out, which means that gas escaping from inside the component is accumulated over time. The leak detector connected to the chamber measures the amount of the accumulated tracer gas for the leak flow rate calculation.

Helium Mass Spectrometer Leak Detection

Helium is chosen as a tracer gas because it penetrates small leaks rapidly. It is an inert gas, non-flammable and present in the atmosphere only in minor quantities (5 ppm).

Detection by mass spectrometer depends on the separation of helium from other gases under vacuum. The tested component is evacuated and charged with helium. The accumulation chamber is evacuated as well. Once the required vacuum level is reached, the leak detector can measure the quantity of helium contained in the accumulation chamber. Correction equations take into account gas viscosity and density. Typically a helium leak detector can measure leaks in the range of 10^{-5} to 10^{-12} Pa m³/s, meaning less than 1 g/yr when converted in leak flow rates of current refrigerants. It should be pointed out that outgassing of all materials should be taken into consideration for pressure vacuum measurements. Moreover, the components require cleaning and degassing by means of vacuum combined with heating or cleaning by hydrogen and nitrogen mixture.

Concentration accumulation under atmospheric pressure

The developed method measures a leak flow rate from the pressurized component to atmospheric pressure where chamber instead of vinyl sheet surrounding it. The advantage of this method is atmospheric pressure inside the accumulation volume (Figure 2.44) representing the real operating conditions. The tracer gas is the refrigerant because of its viscosity. The viscosity of HFC-134a is 30% lower than that of helium. Using refrigerant as tracer gas corresponds to real viscous flow regime of refrigerant [CLODIC 2002]. This testing method is described in detail in the following section.

2.4.2 Concentration accumulation measurement principles

This section describes in detail the leak flow rate determination by measuring the evolution of concentration in an accumulation volume.

2.4.2.1 Concentration measurement methods

In order to measure leak flow rates in the range of 10^{-10} to 10^{-8} mole/s (1 to 10 g/yr for most HFCs), four different types of apparatuses can be possibly used to measure the refrigerant concentration inside control volumes. Those apparatuses are based on different physical principles:

- mass spectrometry,
- gas chromatography,
- infrared spectrophotometer, and
- infrared photo-acoustic spectroscopy.

Mass spectrometry

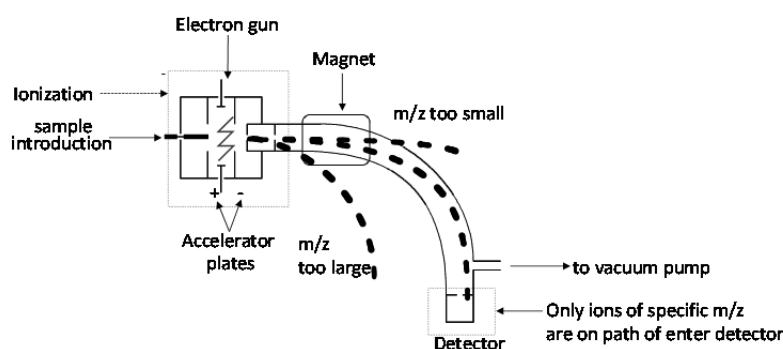


Figure 2.45: Principle of mass spectrometry.

The basic principle of mass spectrometry consists in the determination of molecular mass by manipulating flight path of molecular ion in magnetic field. As shown in Figure 2.45, the gas sample is introduced in a vacuum chamber. An electron gun breaks the molecules into ions that are accelerated by accelerator plates towards the magnet. The magnetic field deflects ions according to their mass to charge ratio m/z . The radius of the ion beam is determined by the ion mass and magnet stress. Therefore, the selected ions are separated and enter the detector. The detector is a mass spectrum that provides molecular weight or even structural information.

Gas chromatography

Gas chromatography is widely used in chemical and processes laboratories. It is a reference method used to measure atmospheric concentration of a tracer gas. The accuracy is one of the best of all methods (± 1 ppb) (10^{-12} to 10^{-11} mole/s). The chromatography technique consists in the separation of molecules according to their molecular structure and molecular composition. Two phases are distinguished (see Figure 2.46) [INT05]:

- Mobile phase: the carrier gas (generally an inert gas like nitrogen or helium) mixed with injected gas sample;
- Stationary phase: a microscopic layer of liquid or polymer coated on an inert solid support called a column.

The mobile phase gas flows through the column installed in a temperature-controlled oven [INT04]. It interacts with the coated walls of the column, making each compound to exit at different time (known as the retention time) and then separation takes place. The retention times allows each compound to be measured individually.

The only difficulty associated with gas chromatography is related to the sampling method. Since the gas sample is mixed with the carrier gas for testing, concentration uncertainties will be introduced when measuring accumulated concentration in the control volume.

Besides, a significant delay could occur between the sampling and the analysis depending on the design of the measurement system.

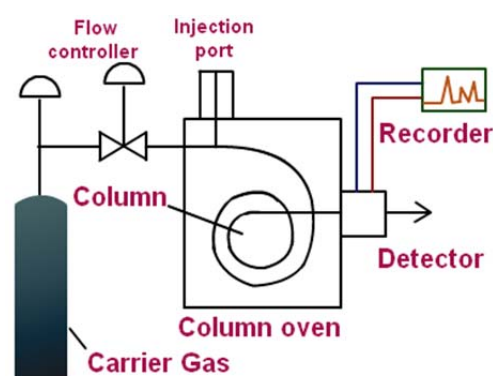


Figure 2.46: Principle of gas chromatography.

Infrared photometry

The principle of the infrared spectrophotometry method uses characteristics of individual gases when absorbing specific infrared wavelength [URAS]. The monitor measures the composition and concentration by analysis of the absorbed wavelengths. The method that uses the infrared rays of all wavelengths radiated from the light source is referred to as "non-dispersive."

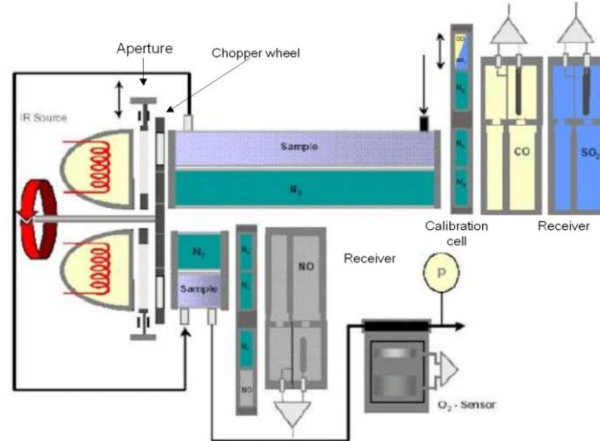


Figure 2.47: IR spectrophotometry Uras-14 measurement principle (by courtesy of ABB).

Figure 2.47 presents the measurement principle of IR spectrophotometry Uras–14. The photometer consists of an infrared source, the emissions of which reach a sample cell via a chopper wheel. The sample cell is in the shape of a tube divided by a wall into sample and reference sides. Two equal-energy infrared beams are directed through these two sides. The measurement effect produced in the receiver is a pressure effect resulting from the chopper frequency, received by a diaphragm capacitor and converted into an electrical signal by a pre-amplifier. The quantity of absorbed infrared radiation is proportional to the absorbing gas concentration. The receiver is a two-layer device. The back of the receiver has an optically transparent window so that any residual radiation can reach a second receiver that is sensitive to a second sample component. By adding a second beam path with an emitter, sample cell, and receivers, the photometer can measure 1 to 4 sample components at the same time. The sensitivity is in the range of 10^{-11} to 10^{-9} mole/s or 0.1 to 10 g/yr.

Infrared photo-acoustic spectroscopy

The photo-acoustic effect is based on the conversion of light energy into sound energy, and a sound-measuring device detects the signal [ROSENCWAIG 1980], [SCHAFER 1999]. The gas to be measured is irradiated by modulated light of a pre-selected wavelength. Radiation absorbed by the molecule from a modulated infrared light beam is efficiently converted into heat energy of the gas molecules, and therefore a temperature and pressure increase in the gas. The pressure will result in an acoustic wave, which can be detected by a sound-measuring device, such as a microphone. The sound pressure, P_{sound} , can be calculated using Equation (2.3).

$$P_{sound} = \frac{K \left(\frac{C_p}{C_v} - 1 \right) \cdot C \cdot I_o}{f_c} \quad (2.3)$$

where, K is a cell and gas dependent constant

C_p and C_v are heat capacities at constant pressure and volume

C is the gas concentration

f_c is the modulation frequency

I_o is the incident light

The IR PAS system presented here, named Innova-1314, is optimized for the quantitative detection of the gas concentration [VECHT 2006]. As illustrated in Figure 2.48, a heated nickel-chrome wire is used as its infrared radiation source. The light from the source is focused by an ellipsoidal mirror, modulated with a mechanical chopper, which pulsates it, and passes through one of the optical filters in the wheel before entering the photo-acoustic gas cell. The filter allows the irradiation of the specific gas with the exact wavelength it absorbs best.

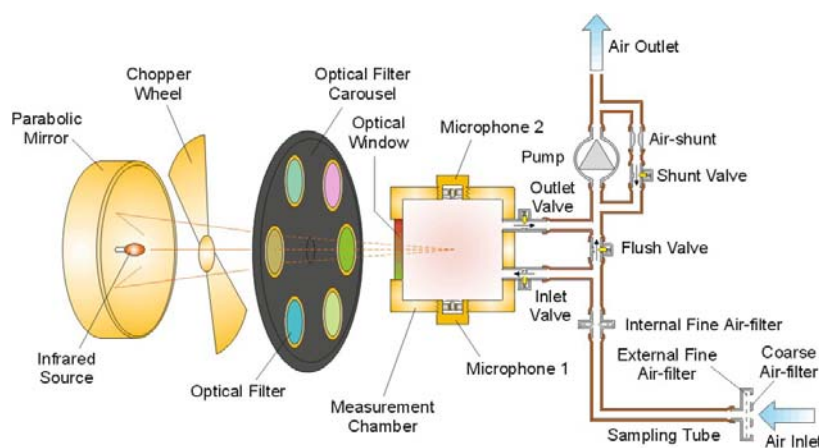


Figure 2.48: PAS Innova-1314 Measurement principle (by courtesy of Innova).

The pump draws a sample from the sampling point through the air-filter to flush out the “old” sample in the measurement system and replace it with a new sample. The “new” sample is hermetically sealed in the analysis cell by closing the inlet and outlet valves. The IR radiation is absorbed by the gas and generates heat and pressure variations in the closed cell. A pair of microphones mounted in the cell walls measures this acoustic signal. By selecting an appropriate resonant mode of opposite phase, the difference signal of the two microphones results in a doubling of the signal amplitude and noise reduction. The electrical signals from the microphones are amplified and added together before being sent to an analogue-to-digital converter. The digital signal is then converted to the concentration of the monitored gas sample present in the cell. The filter wheel turns so that light is transmitted through the next optical filter, and the new signal is measured.

2.4.2.2 Comparison between different detection methods

Accuracies of the different techniques are indicated in Table 2.5.

Table 2.5: Accuracies of different apparatuses.

Apparatuses	Mass spectrometer	Gas chromatography	Infrared photo-acoustic spectroscopy	Infrared spectrophotometry
Accuracy	± 1 ppb	± 1 ppb	± 0.01 ppm	± 0.5 ppm
R-134a sensitivity	0.01 to 0.1 g/yr	0.01 to 0.1 g/yr	0.05 to 1 g/yr	0.1 to 1 g/yr

Since the refrigerant leaks occur under ambient atmospheric pressure and flows are characterized by a viscous regime, the vacuum measurement by mass spectrometry is less adequate than atmospheric one because the flow regime is molecular. Gas chromatography, IR spectrophotometer, and IR Photo-acoustic are the three methods that can be used at atmospheric pressure. Gas chromatography introduces measuring uncertainty because of the sampling method. IR spectrophotometry and IR photo-acoustic are two powerful techniques used to measure small absorptions and can be applied to detect tracer gases in ambient air at atmospheric pressure.

Therefore, two infrared detection methods (IR spectrophotometer and IR photo-acoustic) are chosen for leakage quantification.

Comparison between the IR spectrophotometer (Uras-14) and IR photo-acoustic (Innova-1314)

The Center for Energy and Processes of Ecole des Mines (ARMINES) is equipped with both gas analyzers (IR spectrophotometer and IR photo-acoustic) that present high accuracy, reliability, and stability. Table 2.6 presents some comparisons of IR spectrophotometer (ABB Uras-14) and IR PAS (Innova 1314) specifications.

Table 2.6: Comparison between IR spectrophotometer and IR PAS.

Specification	Concentration measurement	
	IR spectrophotometer (Uras-14)	IR photo-acoustic (Innova –1314)
Gas sampling	Gas sampling at atmospheric pressure	
Calibration	Zero and span gas calibration with gas mixture & automatic calibration by means of internal calibration cell	Zero and end point calibration with gas mixture
Cross-compensation	Yes	
Measurement cell volume	Around 40 milliliters	3 milliliters
Measurement cell status	Open	Closed
Operation mode	Continuous scan	Step scan and nearly continuous scan
Response-time	60~120 s	5-20 sec for one gas
Detection limit	0.5 ppm	10 ppb
Stability	≤ 1% of measured value per week	Change in sensitivity at 25°C: <10%/600 yrs
Measuring range	Two ranges: 0-50 ppm, 0-500 ppm	100 000 times of detection limit

As summarized in Table 2.6, both analyzers are suitable for concentration measurement of gas in ambient air at atmospheric pressure and can measure as many samples as necessary. Calibration can be done at least at zero and span gas. Additionally, Uras-14 is equipped with an internal calibration cell for automatic calibration, which is not the case for Innova –1314. Both Uras-14 and Innova-1314 take this interference into consideration. All the cross-compensation factors are calibrated and stored in the monitor during the calibration.

Comparing the detection principle, Uras-14 is especially suitable for the continuous-scan mode. For Innova-1314 when each step of scan is done one after the other, the measurement can be considered as nearly continuous. Due to the high power pump of Uras-14, measurement is not limited by the distance between the accumulation volume and the gas analyzer, which is not the case of Innova-1314. The volume of the measurement cell Innova-1314 (3 cm³) is smaller than that of the Uras-14 (40 cm³). Because of its volume, the Innova-1314 cell can be swept quickly, which leads to short response time.

According to technical data, Innova-1314 offers higher sensitivity (0.5 ppm for Uras-14 and 10 ppb) for concentration detection. However, because of the limit of resolution (1%) of Innova-1314, it is better to perform low concentration measurement with Innova-1314. For long test period with rapid increase of concentration, Uras-14 is proved more convenient experimentally.

More extended comparison has been made not only theoretically but also experimentally by I. Morgado for the development of leak standard [MORGADO 2008], [MORGADO 2010]. Based on

the operating principle, the photo-acoustic detection is more direct than the spectrophotometer. Microphones used in the IR photo-acoustic to detect the acoustic pressure generated by gas are extremely linear in a wide range of sound pressure. Their detection limits are defined as twice the detection limit of the pressure sensor, which is about 1 μPa . For HFC-134a, a sound pressure around 1 μPa corresponds to a concentration detection limit around 15 $\text{nmol}\cdot\text{mol}^{-1}$. However, for the spectrophotometer, the pressure sensor is not linear. The signal is converted numerically and linearized. In terms of measuring environment, thus, the spectrophotometer seems to be more efficient to attenuate the noise signal. A series of experimental data show that, at low concentrations, the repeatability and linearity are about 10 times better than that of the spectrophotometer.

In summary, for very precise laboratory measurements, the recommendation is to use infrared photo-acoustic systems. For industrial control, infrared spectrophotometry is suitable because it is sufficiently accurate and robust enough to detect leak flow rates lower than 1g/yr.

3 Leak flow rate (LFR) measurement method

3.1 Testing method based on concentration accumulation

Based on the fact that the measurement of concentration is made under atmospheric pressure, two infrared detection techniques described previously are used. For a constant leak flow rate in an accumulation volume, the concentration increases proportionally with time. The leak flow rate (LFR) is calculated [CLODIC 1998], [CLODIC 2004], [CLODIC 2008] according to Equation (2.1).

$$\dot{m}_{\text{HFC-134a}} = M_{\text{HFC-134a}} \cdot \frac{\partial n_{\text{HFC-134a}}}{\partial t} \quad (3.1)$$

Where,

$$n_{\text{HFC-134a}} = n_{\text{total}} \cdot C = \frac{P_{\text{amb}} \cdot V_{\text{accum}}}{R \cdot T_{\text{amb}}} \cdot C \quad (3.2)$$

The mass flow rate is the product of molar mass and the derivative of the number of moles n of HFC-134a along the time in the test chamber. The ideal gas law is used to take into account the small variations of pressure and temperature inside the test chamber. According to Equation (2), the following parameters need to be determined for leak flow rate calculation: the accumulation volume of the test chamber V_{accum} , the temperature T_{amb} and the pressure P_{amb} inside the test chamber, the evolution of concentration along the time.

As shown in Figure 3.1, the measurement system is composed of an accumulation volume at atmospheric pressure where the component to be analyzed is installed and connected to a HFC-134a boiler generating a given level of pressure inside the component. For system measurement, the operation becomes simpler because the refrigerant is directly charged in the system. Temperatures of the component and the ambient air are controlled by heat resistance and fans, which ensure that the component temperature is always above the saturated value of HFC-134a at the test pressure.

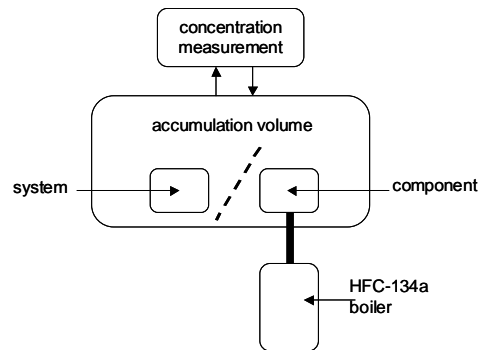


Figure 3.1: Principle of the testing method.

The concentration analyzer is connected to the accumulation volume by a closed circuit and measures continuously the accumulated concentration of HFC-134a inside the volume. Knowing:

- the volume of the accumulation volume,
- the time,
- the concentration at each time step, and
- using Equations (3.1) and (3.2),

the leak flow rate can be calculated.

3.2 Testing protocol

The test protocol [YU 2010] for leak flow rate measurements is described step by step in Figure 3.2

Step 1: Calibration of the test chamber

The uncertainty of the LFR is directly related to the uncertainties on the free volume of the test chamber. First the volume is calculated based on the geometric descriptions. Then a standard

calibrated leak (see Figure 3.4), calibrated on a specific test chamber, is installed inside the test chamber to be calibrated.

$$V_{accum} = \frac{\dot{m}_{HFC-134a}}{\frac{M_{HFC-134a} P_{amb}}{RT_{amb}} \frac{\partial C}{\partial t}} \quad (3.3)$$

Figure 3.5 gives an example of calibration of the accumulation volume. The calibrated leak is measured at constant temperature of 26°C. As indicated in the figure, all parameters such as temperature, pressure, and concentration inside the test chamber are recorded at each time step. The leak flow rate of calibrated leak is obtained as 51.1 g/yr. The accumulation volume can be obtained by reverse calculation of the mass flow rate, which is expressed by Equation (3.3) and consequently its uncertainty is established, which will be discussed in the following section.

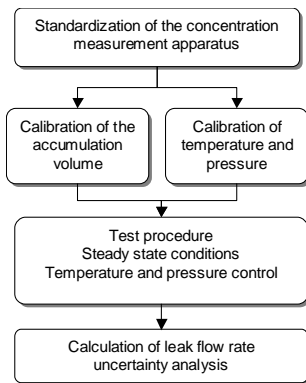


Figure 3.2: Standardized Flowchart of test protocol.



Figure 3.3: Standardized gas of HFC-134a/N₂.



Figure 3.4: HFC-134a calibrated leak.

Step 2: Calibration of temperature and pressure sensors

As shown in Equation (3.3), both temperature and pressure values inside the test chamber contribute to the LFR value. Before installation in the test bench, temperature and pressure sensors are carefully calibrated. The accuracy of both sensors is established through their calibration, which will be discussed later on.

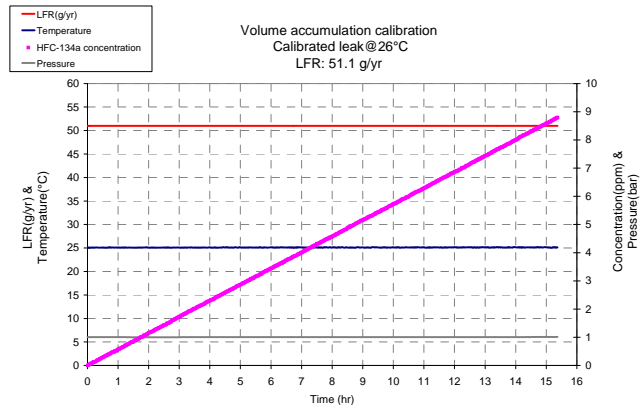


Figure 3.5: Volume calibration data.

Step 3: Testing procedure

After installation of the test sample, the test chamber is closed and then rinsed by a reference gas (artificial air: 80% N₂ + 20% O₂) in order to exclude all possible extraneous particles and guarantee the accuracy of measurement. The pressure is kept at atmospheric pressure. The temperature is maintained constant as well as during the test period. At each time interval, concentration, temperature, and pressure are recorded by the data acquisition system. Tests can be performed either at a single temperature and pressure or at several temperatures and pressures. It is better to use at least three measurement points in order to verify the LFR variations according to saturating pressures.

Step 4: Calculation of leak flow rate

Based on Equations (3.1) and (3.2), the leak flow rate is calculated and the measurement uncertainty is established. Estimation on the uncertainty of leak flow rate test plays an important role, which indicates the reliability of a measurement, so that we will focus on the uncertainty analysis.

Uncertainty analysis of LFR measurement

Based on the principle of indirect measurements from the propagation of distributions, the uncertainty of leak flow rate is achievable [GUIDE 1993]. Since the temperature and pressure are maintained constant during the test, the leak flow rate of the component under test can be calculated according to Equations (3.1) and (3.2). All these uncertainty sources and their influences will be analyzed based on the experimental data [YU 2008].

The functional relationship between the leak flow rate (\dot{m}) and input quantities

($T_{amb}, P_{amb}, V_{accum}, \frac{\partial C}{\partial t}$) is given by Equation (3.4).

$$\dot{m} = f(x_i) = f(T_{amb}, P_{amb}, V_{accum}, \frac{\partial C}{\partial t}) \quad (3.4)$$

The total uncertainty of the leak flow rate is a combination of 4 uncertainty components. By applying the law of propagation, the combined standard uncertainty of the mass flow is written in Equation (3.5):

$$u(\dot{m}) = \sqrt{\left(\frac{\partial \dot{m}}{\partial V_{accum}}\right)^2 u^2(V_{accum}) + \left(\frac{\partial \dot{m}}{\partial T_{amb}}\right)^2 u^2(T_{amb}) + \left(\frac{\partial \dot{m}}{\partial P_{amb}}\right)^2 u^2(P_{amb}) + \left(\frac{\partial \dot{m}}{\partial C / \partial t}\right)^2 u^2(\partial C / \partial t)} \quad (3.5)$$

Therefore, the standard relative uncertainty is calculated according to Equation (3.6).

$$\frac{u_{\dot{m}}}{\dot{m}_{HFC-134a}} = \sqrt{\left(\frac{u_{V_{accum}}}{V_{accum}}\right)^2 + \left(\frac{u_{T_{amb}}}{T_{amb}}\right)^2 + \left(\frac{u_{P_{amb}}}{P_{amb}}\right)^2 + \left(\frac{u_{\partial C / \partial t}}{\partial C / \partial t}\right)^2} \quad (3.6)$$

The accumulation volume consists of two parts: the free volume of the test chamber before installation of a system/component and the volume of the system/component, calculated by Equation (3.7).

$$V_{accum} = V_{FreeVolume} - V_{system / component} \quad (3.7)$$

The free volume of the test chamber is determined using a calibrated leak (Figure 3.4). The obtained leak flow rate value helps to calculate the free volume. This calibration step leads to an uncertainty of about 6%. Moreover, the volume of the system/component can only be obtained by geometrical measurement of all components, some of which include many complex parts. As a result, its uncertainty rises up to 20%. Nevertheless, the uncertainty of this part is negligible compared to the huge free volume inside the test chamber. As demonstrated in Equation (3.8), the relative combined standard uncertainty of the accumulation volume is 6%.

$$\frac{u_{V_{accum}}}{V_{accum}} = \frac{\sqrt{u_{V_{FreeVolume}}^2 + u_{V_{component}}^2}}{V_{accum}} = 0.06 \quad (3.8)$$

Figure 3.6 shows the uncertainty contributions on leak flow rate measurement. It can be observed that the contribution of the accumulation volume to the overall uncertainty is by far the largest, which is followed by the pressure in the cell. Moreover, with large sample sizes the contribution of $\partial C / \partial t$ is relatively small.

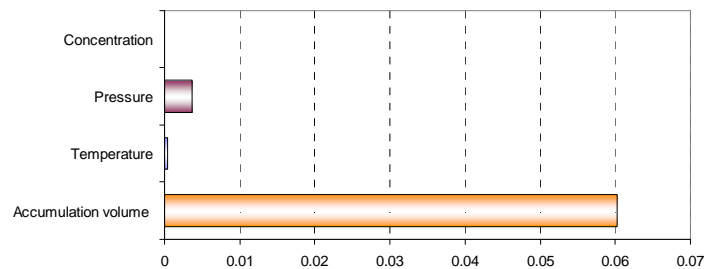
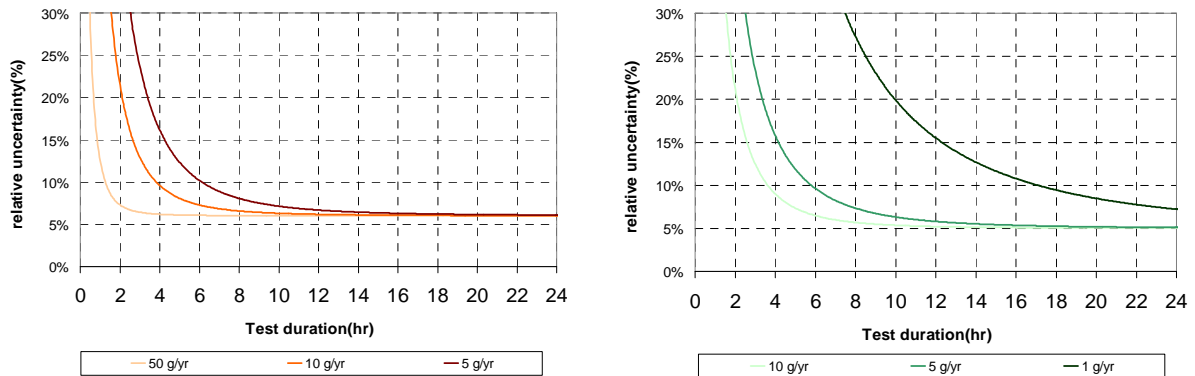


Figure 3.6 : Uncertainty contributions on leak flow rate measurement.

The uncertainty associated to concentration evolution depends on the sample size on standard uncertainty of the flow rate. Longer test duration leads to more concentration samples, which reduces the standard uncertainty. Test duration is related to the sensitivity of the measurement apparatus and to the size of the control volume. The larger the volume, the longer the raise in concentration.



(a) System test bench

(b) Component test bench

Figure 3.7: Relative uncertainty of LFR vs. test duration

Figure 3.7 shows the relative uncertainty of leak flow rate as a function of test duration (120 s for each interval step) with the highest standard deviation of 0.10 (obtained from measurement data of analyzer). When the leak level ranges from 5 to 50 g/yr, in spite of the standard deviation of the regression, it is useless to perform more than 24-hour tests because the relative uncertainty becomes negligible compared to the contribution of the volume uncertainty. For the component test bench, the test chambers are smaller than that of the system, so the relative uncertainty is smaller than that of system tests and can be managed in the range of 5%.

3.3 Test benches for systems and components

The development of a test bench for components started in early 1995 at the CEP-Paris. A second generation test bench has been realized in 1998 equipped with an infrared spectrophotometer. The third generation consists of a system level test bench and component test benches using IR spectrophotometer and IR photo-acoustic. These test benches include three main components [CLODIC 2007]:

- **The system/component to be tested;**
- **The accumulation volume,** where the refrigerant concentration is accumulated and measured;
- **The analyzer,** used to measure the refrigerant concentration in the accumulation volume.

3.3.1 Description of the system test bench

Figure 3.8 presents the test bench for leak flow rate tests of systems in standstill mode [YU 2008], [YU 2010]. The system to be tested (1) is charged with its original HFC-134a charge. Once installed inside the test chamber, it is heated and maintained at the required temperature by an electric heating resistance (2) associated a powerful fan (1500 m³/hr) to ensure homogeneous temperature and concentration distribution inside the test chamber (3). The constant temperature inside the accumulation volume allows the control of the corresponding saturation pressure. In order to reduce the control volume, stainless leak tight cylinders (4) are installed inside allowing accelerating the raise in concentration and so limiting the measurement duration for a given accuracy. Only two circuits are connected to the test chamber:

- the artificial air (80% N₂, 20% O₂) (7) circuit for rinsing the test chamber before testing, and
- the closed measurement circuit between the concentration analyzer (5) and the test chamber.

The temperature and pressure regulation is automatic and likewise the data acquisition (6) and post treatment.

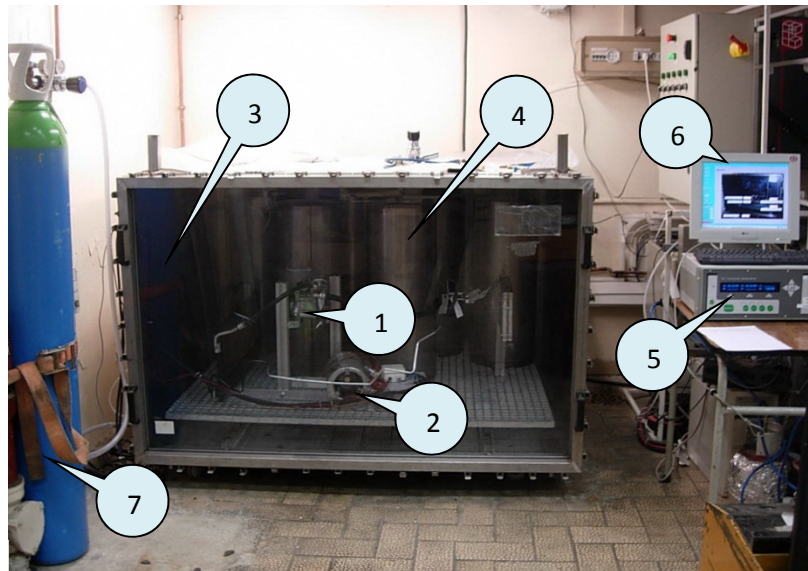


Figure 3.8: Test bench for system measurements.

3.3.2 Description of the component test bench

Figure 3.9 presents the layout of the test bench for leak flow rate measurements of components. The test method for components is identical to the method of test for systems installed in test chamber, except that for the system tests the refrigerant charge is inside the system whereas for component tests, an external refrigerant boiler is mounted outside the accumulation cell. This pressurization circuit is installed outside the accumulation volume and is separately controlled by a heat resistance to define the required pressure.

Each cell can be evacuated by the vacuum pump. After evacuation, the volume is filled up with artificial air at atmospheric pressure. Heating resistance and fans are installed inside the measurement cell to set the component under the required temperature condition. The component can be heated up so that the component temperature is strictly higher than the saturating temperature to avoid any condensation of refrigerant.

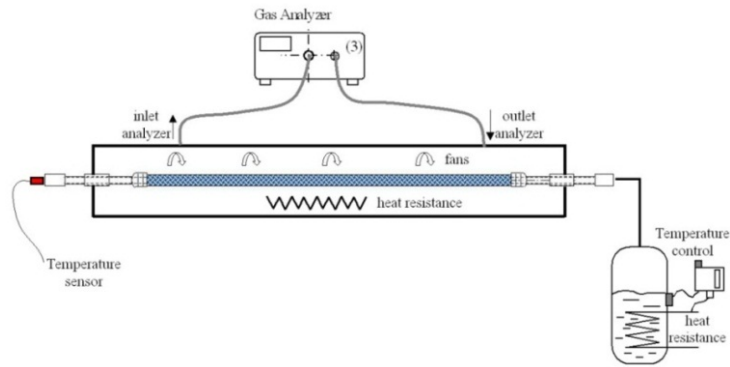
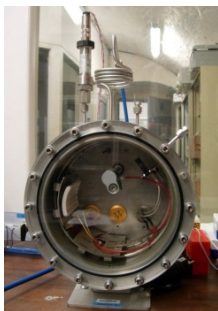
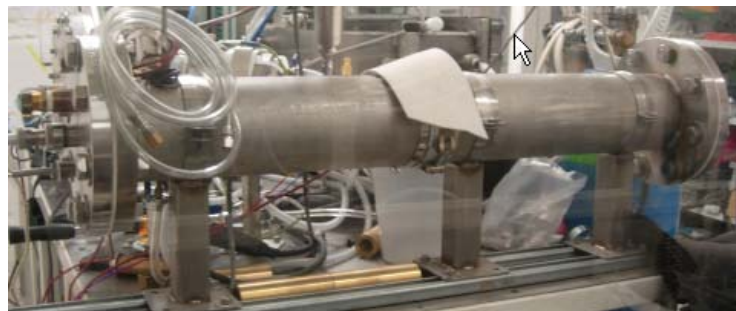


Figure 3.9: Layout of the component measurement test bench.



(a) Cell for fittings



(b) Cell for lines

Figure 3.10: Measurement cells for different types of components.

Once the temperature steady state condition is reached, measurement using the gas analyzer is performed continuously in order to verify that a steady state LFR is reached. The measurement duration depends on the leak tightness of the component as described in § 3.2. Figure 3.10 presents different measurement cells designed for different types of components, such as fittings, hoses, and macro-components like condenser, evaporator, compressor etc.

It should be pointed out that specific preparation is necessary for component before test. One end of the component is closed by welding and the other end is equipped with a tube going through the wall of the accumulation cell. Figure 3.11 gives an example of a prepared component.

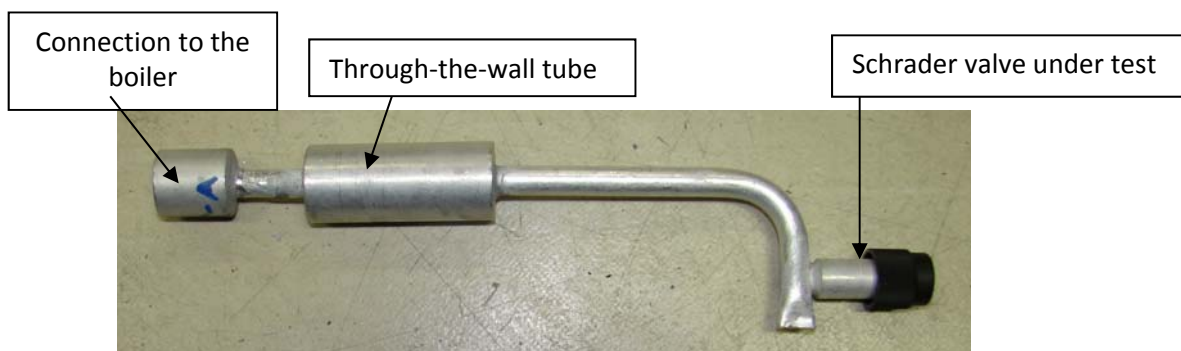


Figure 3.11: Example of component preparation for test.

3.3.3 Investigation of a new charging method

For the purpose to simplify the preparation of components, a new charging system has been developed.

Design of a new charging system

As illustrated in Figure 3.12, the charging system consists of a 250-ml cylinder volume, a VCR™ ball valve, and a Swagelok VCR Metal Gaskets face seal fittings, which is used to connect the test component. The dotted line presents the inside of the accumulation volume. One can see that two supplementary VCR fittings are introduced in the volume: VCR1 and VCR2. Other valves connecting to vacuum pump and refrigerant charge are installed outside of the volume, which does not affect the measurement.

Figure 3.14 shows the details of a VCR assembly. The seal is made when the gasket is compressed by two beads during the engagement of a male nut and a female one. The nut is equipped of test ports at two locations to test leakage easily. Based on data from constructor [INT07], VCR fitting has been helium leak tested to a maximum leak rate of 4×10^{-10} Pa m³/s with silver-plated and copper gaskets. If unplated gaskets are used, the maximum leak rate is 4×10^{-12} Pa m³/s. The unplated-gasket VCR fittings are used for charging the system.

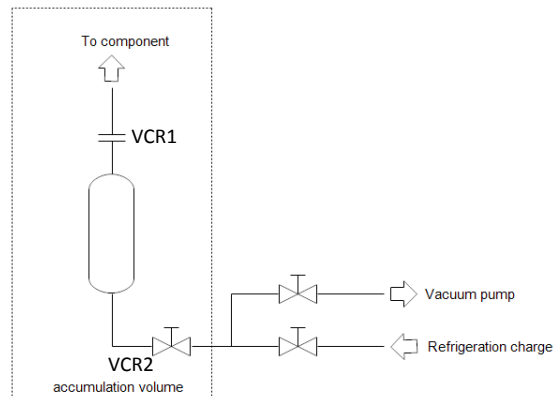


Figure 3.12: Layout of charging system.

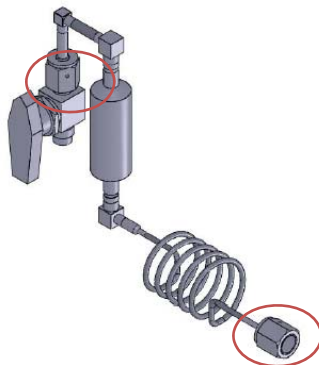


Figure 3.13: 3D scheme of the charging system.

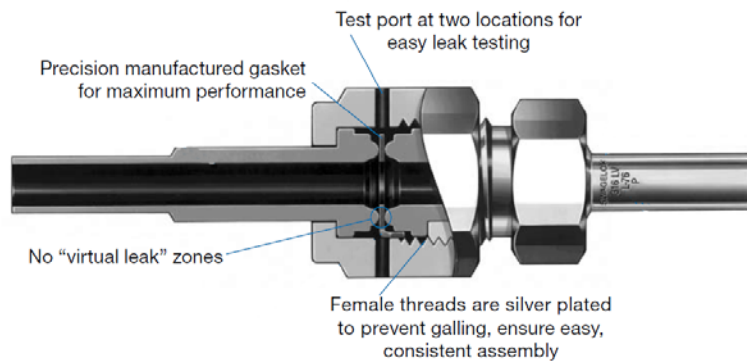


Figure 3.14: VCR assembly (by courtesy of Swagelok).

Characterization of the charging system

Tests have been performed to characterize this charging system. Figure 3.15 shows the charging system installed in an accumulation volume.

Figure 3.16 presents the ambient temperature inside the accumulation volume, the pressure of HFC-134a inside the charging system, and the evolution of the concentration over time. During the test, the temperature is maintained constant using heating resistance and fan inside the accumulation volume. It can be seen that the pressure inside the charging system is constant, which means that the leak tightness of the VCR fittings is so good that they can be neglected. The leak flow rate of the entire charging system is less than 0.001 g/yr. Results show the high leak tightness of the charging system. Once the charging system is characterized, tests have been performed using this charging system.



Figure 3.15: Charging system under test.

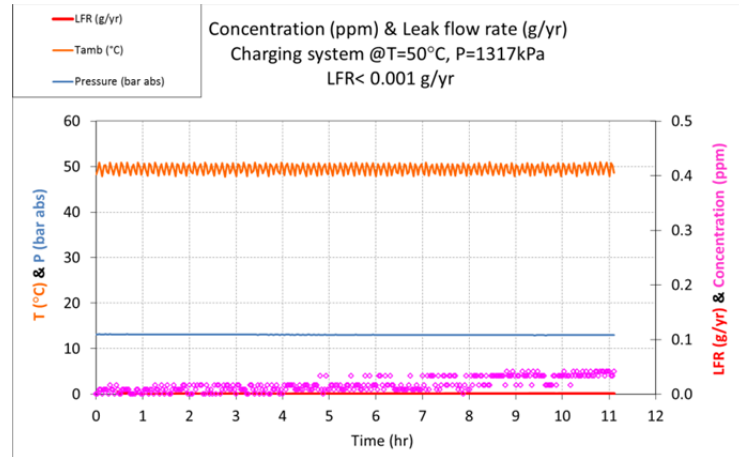


Figure 3.16: Evolution of concentration, temperature, and pressure over time.

4 Leak flow rate tests results

As described in detailed in Section 3, the measurement of concentration is made under atmospheric pressure in an accumulation volume. For a constant leak flow rate, the concentration accumulates in the volume and increases proportionally with time.

The leak flow rate is calculated according to Equation (4.1).

$$\dot{m}_{HFC-134a} = M_{HFC-134a} \cdot \frac{\partial n_{HFC-134a}}{\partial t} \quad (4.1)$$

Where,

$$n_{HFC-134a} = n_{total} \cdot C = \frac{P_{amb} \cdot V_{accum}}{R \cdot T_{amb}} \cdot C \quad (4.2)$$

The mass flow rate is the product of molar mass and the derivative of the number of moles n of HFC-134a along the time in an accumulation volume. The ideal gas law is used to take into account the small variations of pressure and temperature inside the test chamber. According to Equation (4.2), the following parameters need to be determined for leak flow rate calculation: the accumulation volume of the test chamber V_{accum} , the temperature T_{amb} and the pressure P_{amb} inside the test chamber, the evolution of concentration along the time.

Appendix 1 presents the list of components that have been tested among which:

- Schrader valve
- Solenoid valves
- Flare fittings
- Ball valves
- Manual shut-off valves
- Thermal expansion valves (TXVs)
- Electrically operated expansion valves
- Pressure relief valves
- Sight glass
- Filters
- Service valves
- Capillary hose
- Pressure switches

Part of measurement data are presented directly in this section, for helping explanation, and the other part is detailed in Appendix 2.

4.1 Schrader valve

Figure 4.1 shows the cutaway of Schrader valve n°1 to test. Measurements have been carried out at 30, 40, and 50°C based on the testing protocol described in §2.2. As detailed in Table 4.1, leak flow rates at 3 different temperatures are respectively 0.41, 0.69, and 1.08 g/yr.



Figure 4.1: Cutaway view of Schrader valve n°1.

Table 4.1: LFRs of Schrader fitting n°1.

T [°C]	Pressure [kPa]	Leak Flow Rate [g/yr]
30	770	0.41
40	1017	0.69
50	1318	1.08
Parameter k		6.43×10^{-7}

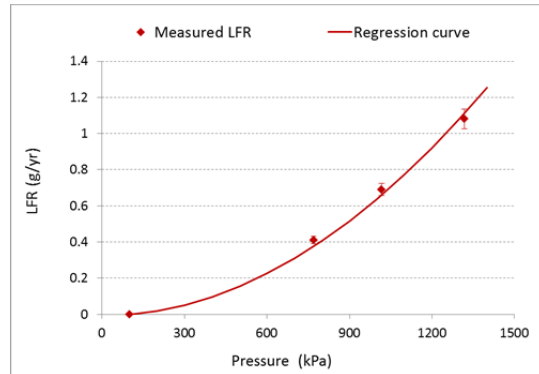


Figure 4.2: Leak flow rate vs. Pressure.

The leaking source consists of two modes: permeation through sealing materials (elastomer) and gas flow in micro channels due to the non-perfect contact between the seal and the metallic parts. According to [YU 2008], both permeation and micro-channel transport phenomena can be approximately regressed by a parabolic function, which is proportional to the difference of the pressure square as shown in Equation (4.3):

$$\dot{m} = k(P_{upstream}^2 - P_{downstream}^2) \tag{4.3}$$

Therefore, the emission law of a component can be established by 3 measurement points. The regression curve of the leak flow rate (shown in Figure 4.2) is calculated using the least square method. Parameter k for this fitting is 6.43×10^{-7} . Therefore, knowing the saturation pressure for a given temperature and parameter k , the leak flow rate of this fitting can be obtained. For example, the leak flow rate is 0.16 g/yr at constant temperature of 16°C (saturation pressure: 540kPa).

4.2 Solenoid valves

Two solenoid valves of same technology have been tested. Only the inlet and outlet connections are different. As shown in Figure 4.13, valve n°1 is connected by brazing tubes. Valve n°2 is equipped with flare ends. Thus, preparation for each valve is different. For brazing ends, one extremity is closed by brazing. For flare ends, a female cap is used to close the component. There are always VCR fittings connected to the other extremity for refrigerant charging.



Figure 4.3: Solenoid valve n°1.



Figure 4.4: Expanded view of solenoid valve.

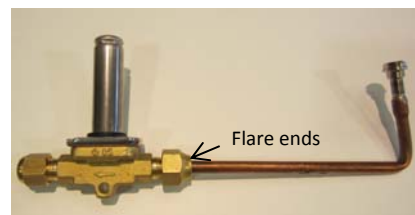


Figure 4.5: Solenoid valve n°2.

According to the test specifications (detailed in IR n°2), before the leak test, the component has been installed in the test chamber. Once evacuated, it has been charged with the HFC-134a and heated up to 50°C. The pre-conditioning period takes two days under this condition. Thereafter, the measurements have been performed at 3 different temperatures: 30, 40, and 50°C. Measurement results are presented below.

In each figure, parameters used for leak flow rate determination are recorded along the time. Table 4.2 summarizes the calculated leak flow rates of the valve at temperatures of 30, 40, and 50°C. Results allow obtaining the regression curve (red line in Figure 4.6) using the method of Least Squares. The relationship between leak flow rate and pressure is based on Equation (4.3) as mentioned in IR n°2:

$$\dot{m} = k(P_{upstream}^2 - P_{amb}^2) \tag{4.3}$$

Where,

$P_{upstream}$ is the refrigerant pressure inside the component

P_{amb} is the ambient pressure

Table 4.2: LFRs of solenoid valve n°1.

T [°C]	Pressure [kPa]	Leak Flow Rate [g/yr]
30	770	0.047
40	1017	0.086
50	1318	0.165
Parameter k		9.0×10^{-8}

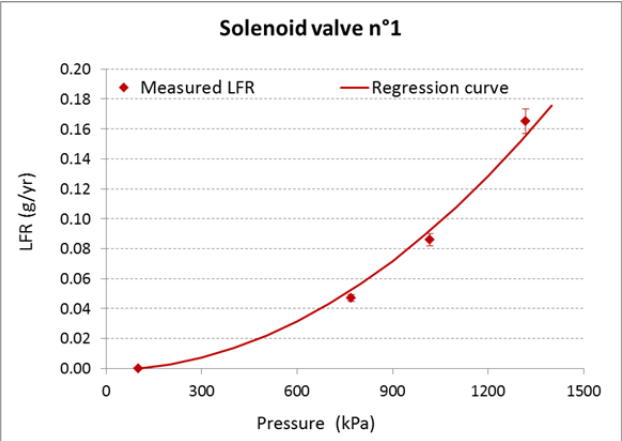


Figure 4.6: Leak flow rate vs. Pressure (Solenoid valve n°1).

Once k has been determined by the regression curve and knowing the saturation pressure for a given temperature, the valve leak flow rate can be easily obtained.

Leak flow rate measurement of Solenoid valve n°2

Solenoid valve n°2 has been tested under the same conditions as solenoid valve n°1. Table 4.3 shows the leak flow rates of valve n°2 that are respectively 0.040 g/yr at 30°C, 0.086 g/yr, and 0.165 g/yr at 50°C. Similar results have been observed for LFRs of valve n°1, which shows a good repeatability of the sealing technique. Moreover, connecting modes (brazing / flare) seem to have no impact on the emission level of this component.

Table 4.3: LFRs of solenoid valve n°2 with flare fittings.

T [°C]	Pressure [kPa]	Leak Flow Rate [g/yr]
30	770	0.040
40	1017	0.086
50	1318	0.165
Parameter <i>k</i>		8.8×10^{-8}

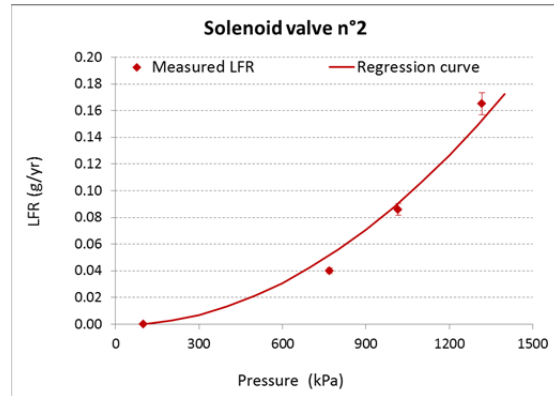


Figure 4.7: Leak flow rate vs. Pressure (Solenoid valve n°2).



Figure 4.8: Solenoid valve n°3.

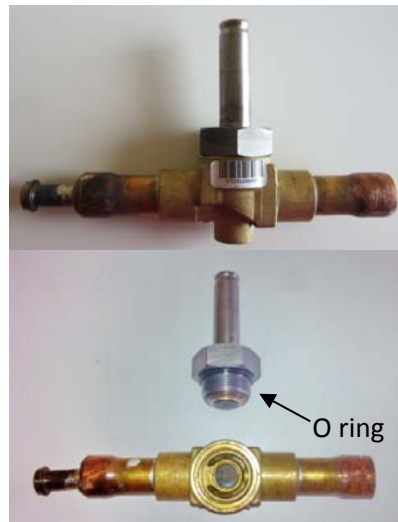


Figure 4.9: Solenoid valve n°4.

Two solenoid valves have been tested. As shown in Figure 4.8 and Figure 4.9, only an O-ring is used as seal. Table 4.4, summarizes measurements of leak flow rates of solenoid valve n°3: 0.07, 0.15, and 0.23 g/yr at 30, 40, and 50°C respectively. The constant *k* used for the leak flow rate calculation at other temperatures is 1.37×10^{-7} . LFRs of solenoid valve n°4 are 0.44, 0.82, and 1.31 g/y and the constant *k* is 7.69×10^{-7} .

Table 4.4: LFRs of solenoid valves n°3 and n°4.

T [°C]	Pressure [kPa]	Solenoid valve n°3 Leak Flow Rate [g/yr]	Solenoid valve n°4 Leak Flow Rate [g/yr]
30	770	0.07	0.44
40	1017	0.15	0.82
50	1318	0.23	1.31
<i>k</i>		1.37×10^{-7}	7.69×10^{-7}

Figure 4.11 and Figure 4.12 present the emission regression curve of each valve as a function of pressure. Comparing results, it can be seen that emission rate is not equal when using similar sealing technology. Figure 4.10 compares the internal diameter of O-ring seals, which are 13 mm for solenoid valve n°3 and 22 mm for valve n°4. Larger diameter leads to higher leak flow rate.

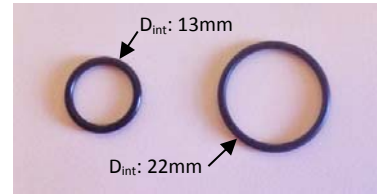


Figure 4.10: O-ring diameters.

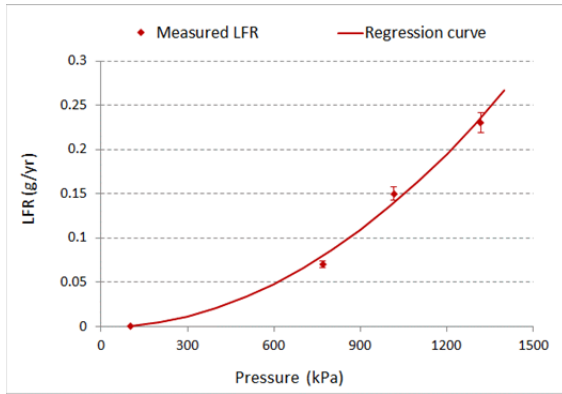


Figure 4.11: Leak flow rate vs. Pressure (Solenoid valve n°3).

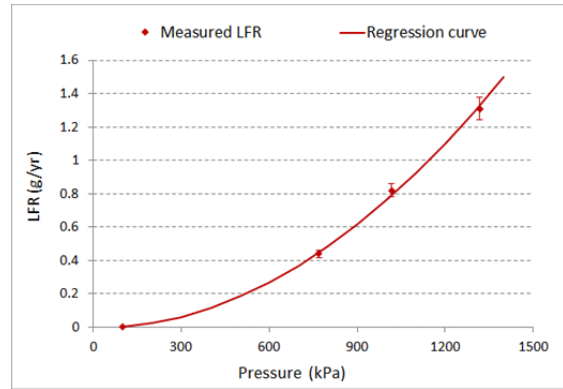


Figure 4.12: Leak flow rate vs. Pressure (Solenoid valve n°4).

4.3 Flare fittings

- Flare fittings n°1 (¼ inch)

Due to the charging system, the preparation of the flare fitting has been simplified. As demonstrated in Figure 4.13, only a VCR fitting is brazed to the extremity of the fitting. The flare fitting has been initially tested without any gasket.



Figure 4.13: Preparation of flare fitting n°1.



Figure 4.14: Leak detected by soap bubble.

As shown in IR n°1, the sealing technique of flare fitting is purely metal to metal seal and is the result of two sloped surfaces coming together. The leak tightness is torque dependent. As shown in Figure 4.14, when 5-Nm torque is applied to the fitting, the leak is so huge that it can be detected by soap bubble spray. By increasing the torque, the leak flow rate decreases significantly. With a torque increase from 8 Nm up to 16 Nm, the measured leak flow rates are 0.003, 0.003, and 0.002 g/yr (see Table 4.5). More tests will be performed to see influences of the temperature and the surface roughness of two contacting metallic parts.

Table 4.5: LFRs of Schrader fitting n°1.

T [°C]	Pressure [kPa]	Torque [Nm]	Leak Flow Rate [g/yr]
50	1318	5	Huge leak
		8	0.003
		12	0.003
		16	0.002

To conclude, this section shows primary leak flow rate measurement results to give some idea of the leak flow rates of a new Schrader valve at 3 temperatures of 30, 40, and 50°C.

- Flare fittings n°2 (3/8 inch) and n°3 (1/2 inch)



Figure 4.15: Flare fitting 3/8 under test.



Figure 4.16: Flare fitting 1/2 under test.

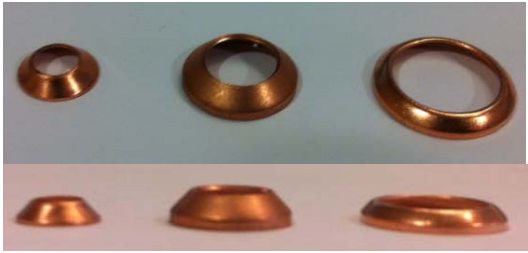


Figure 4.17: Gasket for 3 fitting sizes.

Figure 4.15 and Figure 4.16 show flare fittings n°2 and n°3 corresponding to 3/8 inch and 1/2 inch sizes. For fitting n°2, the fitting needs to be tightened at least by 20 Nm. The leak flow rate reduces from 0.057 g/yr to 0.020 g/yr with a torque increase from 20 Nm up to 30 Nm. Moreover, 40 Nm have been necessary to decrease the leakage level of fitting n°3. Under 20 Nm, the leak can be detected by soap bubbles (see Figure 4.16).

Table 4.6: LFRs of Schrader fittings no. 2 and no. 3.

T [°C]	Pressure [kPa]	Torque [Nm]	Leak Flow Rate [g/yr] no.2	Leak Flow Rate [g/yr] no.3
50	1318	10	Huge leak	Huge leak
		20	0.057	Huge leak
		30	0.020	12.8
		40	NC	0.072

Gaskets used for three fittings are presented in Figure 4.17. It can be seen that the shape of the third gasket (1/2) appears quite different from the others. Based on test results, the leakage levels of flare fittings are quite variable depending on the applied torque, the sizes, and shapes of the fittings. A large size flare fitting requires better mounting and verifying.

4.4 Ball valves

Two ball valves have been tested. Figure 4.18 shows the prepared valve n°1. One extremity is closed and the other side is brazed with a VCR fitting for connection. Valve n°2 has been prepared in the same way (see Figure 4.19). Compared to valve n°1, valve n°2 is equipped with a Schrader fitting. The valve cap has been removed as well in order to see the difference.



Figure 4.18: Prepared ball valve n°1.



Figure 4.19: Prepared ball valve n°2.

Leak flow rate measurement of ball valves n°1 and n°2

Since both valves have been tested at the same time, concentration evolutions for both are presented in one figure (Figure 4.20). The green line presents valve n°1 and the pink one presents

valve n°2. At the end of 10-day measurement at 3 temperatures, the concentration of valve n°1 only increases 2 ppm. For valve n°2, the final point gives about 6 ppm. It can be clearly observed that due to the Schrader fitting and the absence of valve cap, the emission of the valve and the Schrader is slightly higher than the valve itself.

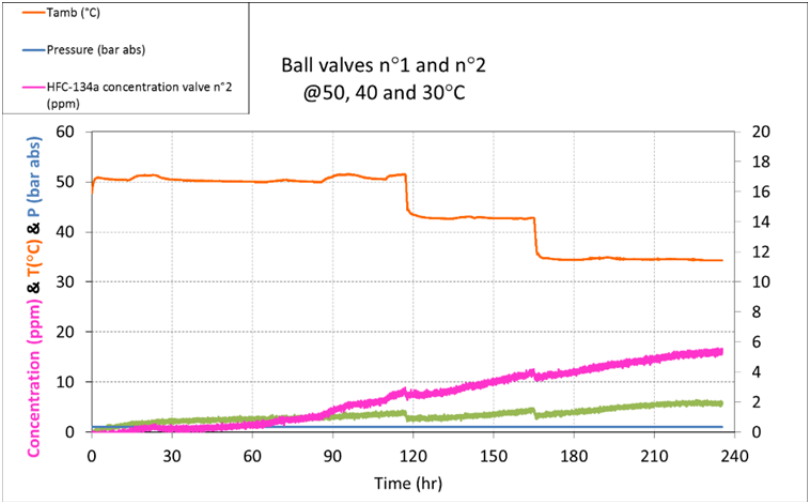


Figure 4.20: Concentration evolution as a function of time.

Table 4.7: LFRs of ball valves n°1 and n°2.

T [°C]	Pressure [kPa]	Leak Flow Rate of ball valve n°1 [g/yr]	Leak Flow Rate of ball valve n°2 [g/yr]
30	770	0.008	0.016
40	1017	0.013	0.021
50	1318	0.018	0.028
<i>Parameter k</i>		1.2×10^{-8}	2.5×10^{-8}

Table 4.7 summarizes the leak flow rates of valves n°1 and n°2. The emission rates of valve n°1 are respectively 0.008, 0.013, and 0.018 g/yr. Those of valve n°2 are 0.016, 0.021, and 0.028 g/yr. As illustrated in Figure 4.21 and Figure 4.22, the emission rate of valve n°2 equipped with a Schrader fitting and without its cap is nearly the double of the simple valve (n°1). Nevertheless, both present quite low leak flow rates.

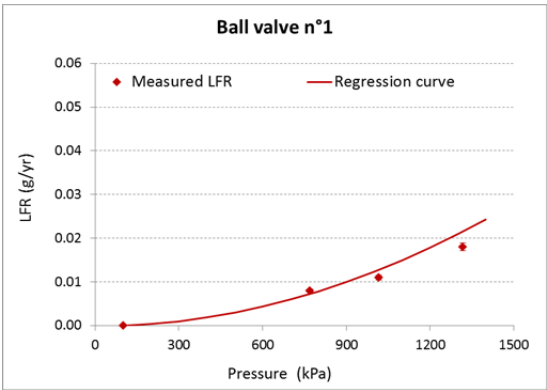


Figure 4.21: Leak flow rate vs. Pressure (Ball valve n°1).

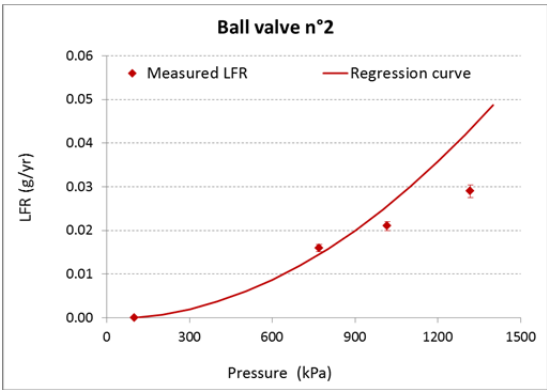


Figure 4.22: Leak flow rate vs. Pressure (Ball valve n°2).

4.5 Manual shut-off valves

Manual shut-off valve n°1 shown in Figure 4.23 has been tested. Figure 4.24 shows the cutaway of valve n°1. It can be seen that the edge of the metallic diaphragm is used as seal. Compression between the cover and the valve body prevents the valve from leaking.



Figure 4.23: Preparation of manual valve n°1.

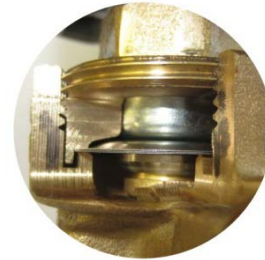


Figure 4.24: Cutaway view of manual valve n°1.



Figure 4.25: Preparation of manual valve n°2.



Figure 4.26: Expanded view of manual valve n°2.

As shown in Table 4.8, the leak flow rate of valve n°1 is 0.040 g/yr at 50°C and 0.029 g/yr at 40°C. Leak flow rates of valve n°2 are quite high: 0.34 g/yr at 50°C and 0.21 g/yr at 40°C.

Table 4.8: LFRs of manual shut-off valve n°1.

T [°C]	Pressure [kPa]	Leak Flow Rate Valve n°1 [g/yr]	Leak Flow Rate Valve n°2 [g/yr]
50	1318	0.04	0.34
40	1017	0.03	0.21

As it can be seen from Figures 4.24 and 4.26 the leak tightness technology is different from one design to the other. As a first evaluation, technology of valve no. 1 seems better than the other. Nevertheless, the levels of leak tightness of both manual valves are acceptable.

4.6 Thermal expansion valves (TXV)

- TXV n°1

Figure 4.27 shows the prepared TXV n°1 to test. This valve uses brazing ends for connection. For preparation, one end is closed by brazing and the other one is brazed to a VCR fitting for charging. Figure 4.28 presents the TXV installed in the accumulation volume during the test. Tests have been carried out at 50, 40, and 30°C after 2-day preconditioning at 50°C.



Figure 4.27: Photo of prepared TXV n°1.

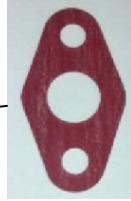


Figure 4.28: TXV n°1 installed inside the accumulation volume.

As given in Table 4.9, leak flow rates of this TXV are 0.016 g/yr at 30°C, 0.030 g/yr at 40°C, and 0.052 g/yr at 50°C. The constant k is 3.7×10^{-8} , which can be used for leak flow rate calculation at other temperatures.

Table 4.9: LFRs of TXV n°1.

T [°C]	Pressure [kPa]	Leak Flow Rate [g/yr]
30	770	0.016
40	1017	0.030
50	1318	0.052
k		3.7×10^{-8}

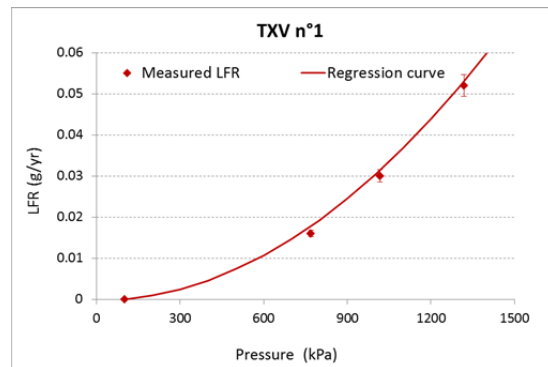


Figure 4.29: Leak flow rate vs. Pressure.

- TXV n°2

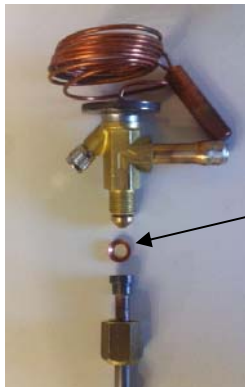


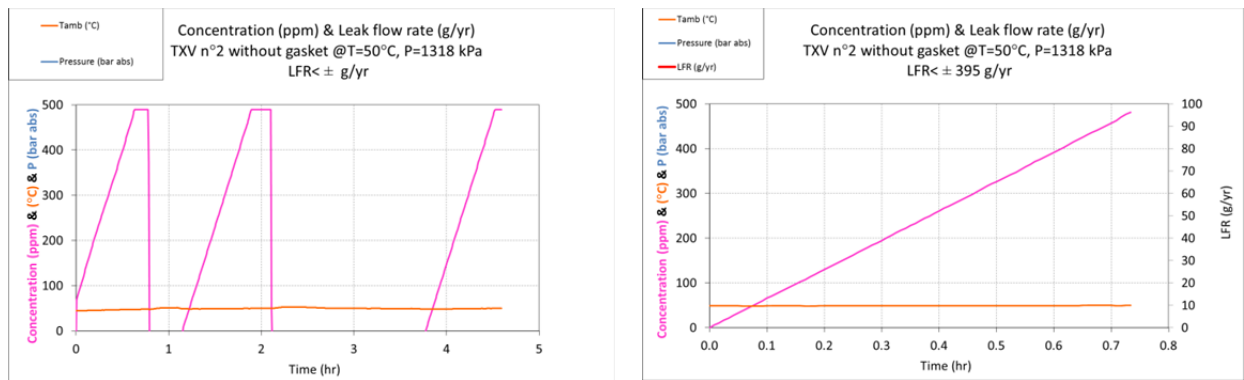
Figure 4.30: TXV n°2.



Figure 4.31: TXV n°3.

Figure 4.30 shows the prepared TXV valve n°2. This valve has been first tested without gasket; huge leak flow rate of 395 g/yr has been obtained. Then the gasket is installed for testing. As given in Table 4.10, the leak flow rate reduces down to 0.003 g/yr. It is obvious that gasket plays an important role for leak tightness.

Leak flow rate measurement of TXV n°2 without gasket



Leak flow rate measurement of TXV n°2 with gasket

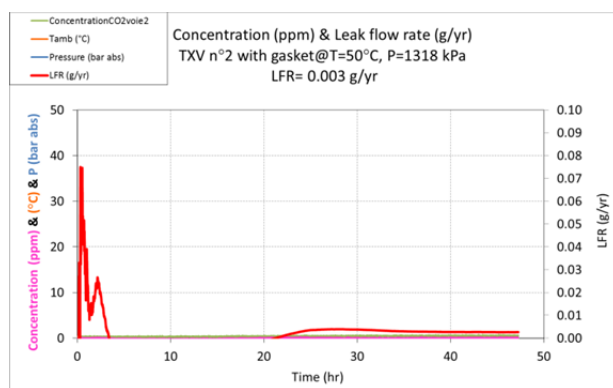


Table 4.10: LFRs of TXV n°2.

T [°C]	Pressure [kPa]	Leak Flow Rate of TXV n°2 Without gasket [g/yr]	Leak Flow Rate of TXV n°2 With gasket [g/yr]
50	1318	395 g/yr	0.003 g/yr

- TXV n°3

TXV valve n°3 has been tested with gasket. Results are presented in Table 4.11. At 40 and 50°C, leak flow rates of this valve are 0.015 g/yr and 0.021 g/yr.

Table 4.11: LFRs of TXV n°3.

T [°C]	Pressure [kPa]	Leak Flow Rate [g/yr]
40	1017	0.015
50	1318	0.021

- TXV n°4

TXV n°4 is a stainless steel thermostatic expansion valves. As shown in

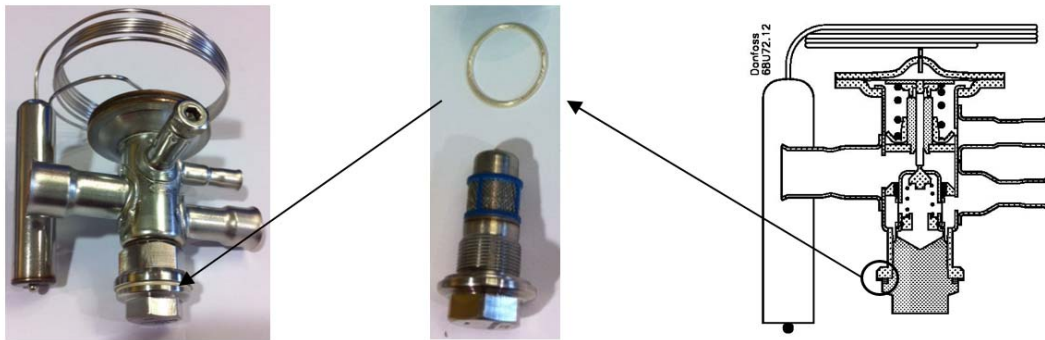


Figure 4.32, the expansion valve is compact, light, and has steel / copper bi-metal connections for brazing. This valve has an interchangeable orifice and adjustable superheat.



Figure 4.32: TXV n°3.

It can be seen in the figure that the leak tightness between the valve body and the orifice is guaranteed by a metal O-ring.

Table 4.12: LFRs of TXV n°4.

T [°C]	Pressure [kPa]	Leak Flow Rate [g/yr]
50	1318	0.013
40	1017	0.008

4.7 Electrically operated expansion valves

Electronically operated valves designed for refrigeration systems are used in conjunction with electronic controllers. Two types of valves have been tested here. Figure 4.33 presents an all welded valve. One end is closed and the other one is connected to the pressure charge fitting. For valve n°2 (see Figure 4.34), the orifice assembly is replaceable. One copper gasket is used as seal.



Figure 4.33: Electrically operated expansion valve n°1.



Figure 4.34: Electrically operated expansion valve n°2.

Table 4.13: LFRs of electrically operated expansion valves n°1 and n°2.

T [°C]	Pressure [kPa]	Leak Flow Rate Valve n°1 [g/yr]	Leak Flow Rate Valve n°2 [g/yr]
50	1318	0.017	0.012
40	1017	0.008	0.006

As shown in Table 4.13 the leak flow rates of valve n°1 is 0.017 g/yr at 50°C and 0.008 g/yr at 40°C. Tests of valve n°2 give 0.012 g/yr at 50°C and 0.06 g/yr at 40°C.

It is clear that the levels of leak tightness of both technologies are quite good and the differences exist but are small.

4.8 Pressure relief valves

Three pressure relief valves as shown in Figure 4.35, Figure 4.36, and Figure 4.37 have been tested. It should be pointed out that beside each relief valve body, Teflon tape is used to seal the connection between the valve and the adapter. Therefore, measured leak flow rates include both leak sources.



Figure 4.35: Photo of prepared pressure relief valve n°1.



Figure 4.36: Pressure relief valve n°2.



Figure 4.37: Pressure relief valve n°3.

After testing new valves, valves have been opened 10 times by charging high-pressure of nitrogen. Measurements are summarized in Table 4.14. For pressure relief valve n°1, before and after pressure relief, leak flow rates are respectively 0.02 and 0.03 g/yr. LFRs of valve n°2 increased from 0.01 g/yr up to 0.04 g/yr. Emission rates of valves n°1 and n°2 increase slightly after pressure relief.

Table 4.14: LFRs of pressure relief valves n°1, n°2, and n°3.

T [°C]	Pressure [kPa]		LFR of pressure relief valve n°1 [g/yr]	LFR of pressure relief valve n°2 [g/yr]	LFR of pressure relief valve n°3 [g/yr]
50	1318	new	0.02	0.01	0.01
		After 10 times relief	0.03	0.04	0.03

Those three pressure relief valves show very good leak tightness even after several openings. No significant differences can be seen from results.

4.9 Sight glass

Two built-in sight glasses have been tested (see Figure 4.38 and Figure 4.39). Connections for n°1 are flare ends and those of sight glass n°2 are brazing ends. During the test, one end is closed and the other one is connected to a VCR fitting as usual.



Figure 4.38: Sight glass n°1 with flare ends.



Figure 4.39: Sight glass n°2 with brazing ends.

Leak flow rate measurement

- T = 50°C (Sight glass n°1)

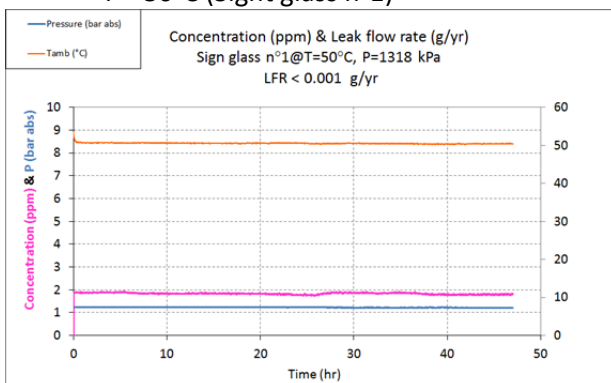


Figure 4.40: Concentration evolution vs. time.

- T = 50°C (Sight glass n°2)

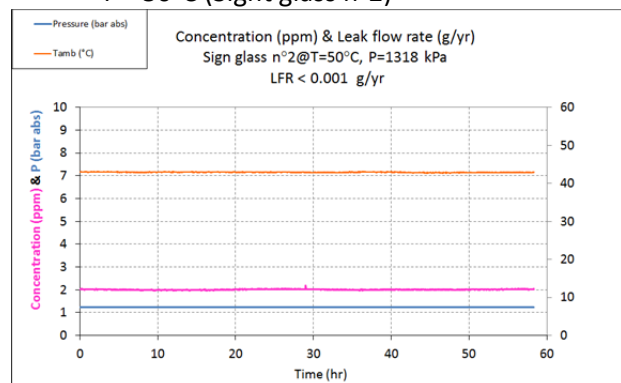


Figure 4.41: Concentration evolution vs. time.

As illustrated in Figure 4.40 and Figure 4.41, the concentration inside the accumulation volume remains nearly constant along the time. Calculated leak flow rates of the both components are lower than measurement precision 0.001 g/yr. Conclusion can be drawn from the results that the emission rates of both hermetically sealed sight glasses are low enough to be neglected.

Table 4.15: LFRs of sight glasses n°1 and n°2.

	T [°C]	Pressure [kPa]	Leak Flow Rate [g/yr]
Sight glass n°1 (flare ends)	50	1318	<0.001
Sight glass n°2 (brazing ends)	50	1318	<0.001

As shown in Figure 4.42: Sight glass n°3, sight glass n° 3 uses Teflon ring as seal. It has been tested by applying different torques to see the influence. This component has been tested at 50°C applying 10, 15, 20, and 25 Nm torques. Measurements are presented Table 4.16.

When 10 Nm is applied to the component, a high value of leakage has been observed: 240 g/yr. By increasing the torque from 10 Nm to 15 Nm, the leak flow rate decreases significantly, down to 8.6 g/yr. 20 Nm and 25 Nm torques lead to relatively low leak flow rate of 0.28 and 0.17 g/yr.



Figure 4.42: Sight glass n°3.

Table 4.16: LFRs of sight glass n°3.

T [°C]	Pressure [kPa]	Leak flow rate (g/yr)			
		10 Nm	15 Nm	20 Nm	25 Nm
50	1318	240	8.6	0.28	0.17

Results lead to the following conclusion: Teflon O-ring sealing technology is quite sensitive to torque. Careful attention should be paid for assembly; otherwise, the sight glass will be significant contributor to leakage.

4.10 Filters/driers



Figure 4.43: Cutaway view of filter n°1.



Figure 4.44: Photo of prepared filter n°1.

A filter using the similar Teflon seal ring has been tested. As summarized in Table 4.17, leak flow rates are respectively of 0.07, 0.12, and 0.18 g/yr at temperatures of 30,40, and 50°C.

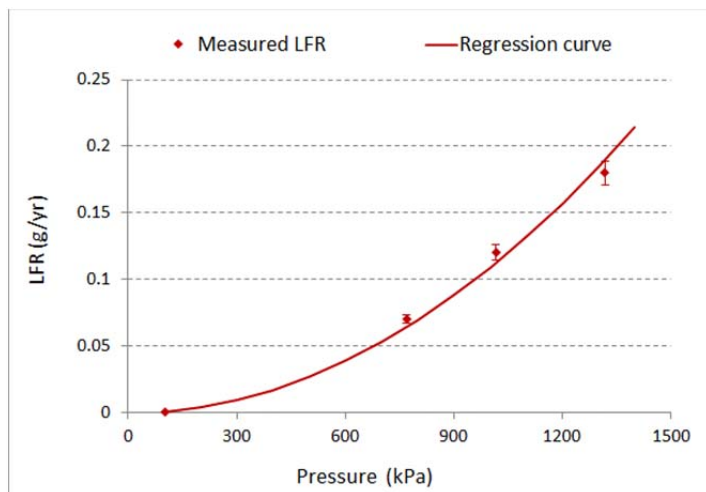


Figure 4.45: Leak flow rate vs. Pressure (Filter n°1).

Table 4.17: LFRs of Filter n°1.

T [°C]	Pressure [kPa]	Leak Flow Rate [g/yr]
30	770	0.07
40	1017	0.12
50	1318	0.18



Figure 4.46: Filter n°2.



Figure 4.47: Filter n°3.

As shown in Figure 4.46 and Figure 4.47, both filters n°2 and n°3 are one-body hermetic. Filters are delivered with ¼-inch flare connections. For leak flow rate measurements, one end is closed by a cap and the other end is connected to the charging system. Based on Table 4.18, leak flow rates of both hermetic filters are quite low and no significant difference can be seen in results.

Table 4.18: LFRs of Filters n°2 and n°3.

	Temperature [°C]	Pressure [kPa]	Leak Flow Rate [g/yr]
Filter n°2	50	1318	0.003
Filter n°3	50	1318	0.004

4.11 Service valves

- Angle service valve n°1

Service valve n°1 shown in Figure 4.48 has been tested. It can be seen from the cutaway view that 4 seals used. As given in Figure 4.49, good leak tightness has been observed. Only 0.004 g/yr is obtained at 50°C.

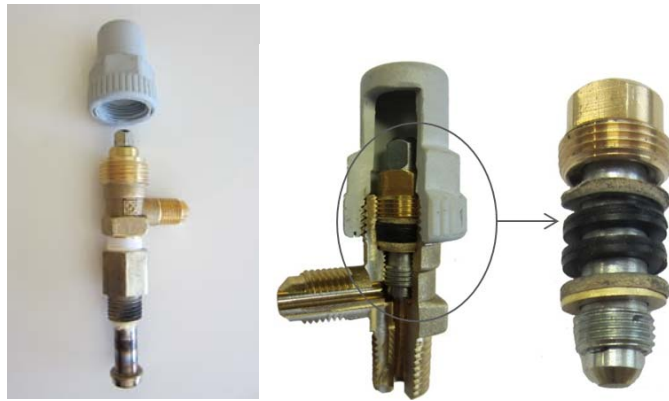


Figure 4.48: Service valve n°1.

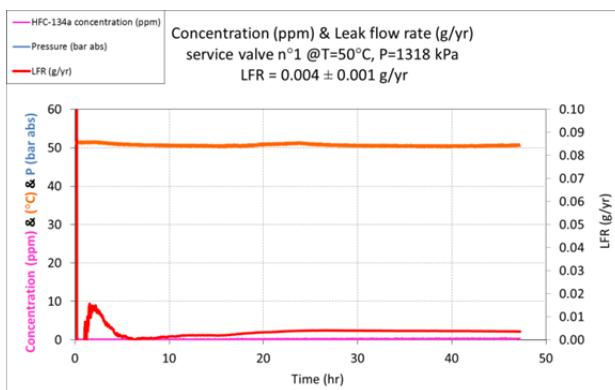


Figure 4.49: Concentration evaluation vs. time.

Table 4.19: LFRs of service valve n°1

T [°C]	Pressure [kPa]	Leak Flow Rate [g/yr]
50	1318	0.004

- Angle service valve n°2

Service valve n°2 has been prepared as shown in Figure 4.50. Figure 4.51 presents a picture of the valve installed inside the test chamber and under test. As illustrated in the figure, the valve is tested without the cap. The valve has been measured new and after 10 times opening in order to analyze the emission difference.



Figure 4.50: Prepared service valve n°2.



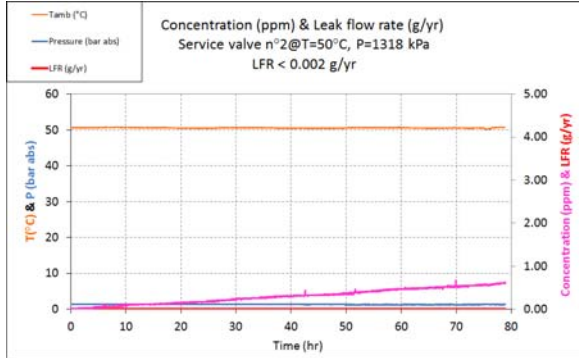
Figure 4.51: Service valve under test.

As observed in Table 4.20, before and after opening, the leak flow rate of this valve is in the range of 0.002 and 0.003 g/yr. One can conclude that, moderate operation does not change the emission level of the valve that remains quite low.

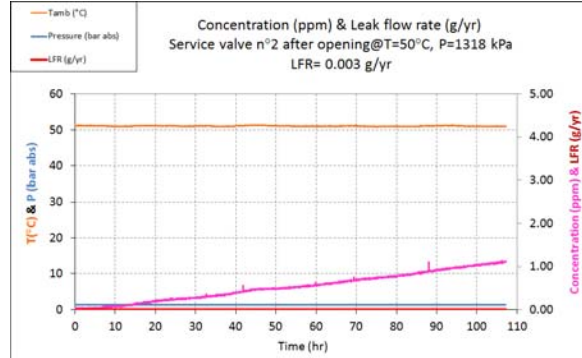
Table 4.20: LFRs of service valve n°2.

T [°C]	Pressure [kPa]	Leak Flow Rate of service valve n°2 [g/yr]	
		New	After opening
50	1318	0.002	0.003

- n°1: T = 50°C (new)



- n°2: T = 30°C (after opening)



- 3-way Rotolock service valves

The Rotolock valves are commonly used to isolate the compressor or the receiver from the refrigeration system and to provide quick access to the system pressure. Using these valves allows the reduction of the service repair time. Two 3-way Rotolock service valves of the same technology (see Figure 4.52) have been tested.



Figure 4.52: Prepared service valves n°3 and n°4.

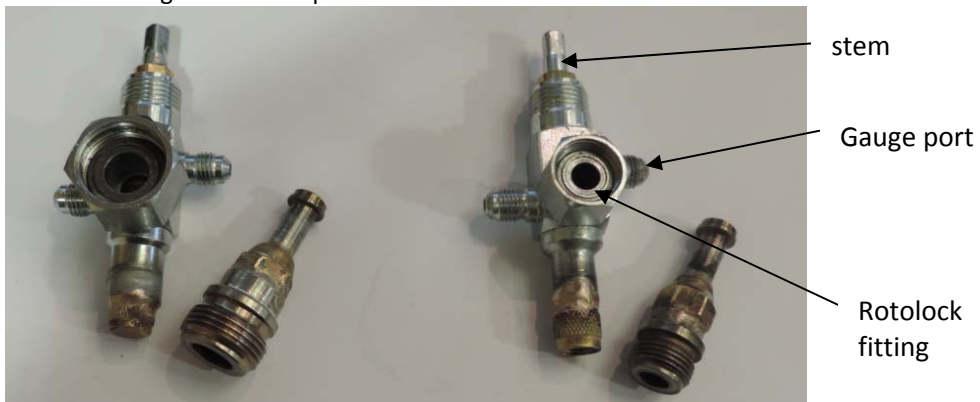


Figure 4.53: Prepared service valves n°2 and n°3.

As shown in Figure 4.53, leak sources of those valves come from:

- The leak tightness between the stem and the valve body

- Two gauge ports
- The Rotolock fitting

Figure 4.53 shows that for valves n°2 and n°3, only the size of the Rotolock fitting is different. Valve n°3 uses a 3/8 Teflon ring and valve n°4 a ¼ Teflon ring.

Table 4.21: LFRs of Rotolock service valves n°3 and n°4.

	T [°C]	Pressure [kPa]	Leak Flow Rate [g/yr]	Leak Flow Rate after handling [g/yr]
Service valve n°3	50	1318	0.025	0.021
Service valve n°4	50	1318	0.017	Not tested

- Rotolock fitting n°5

Rotolock fitting n°5 is equipped with a ½” Teflon ring. It should be pointed out that this Rotolock fitting is a used one and the surface of both male and female parts are not clean and some kind of metal oxidation product can be observe on the surface of connection parts. The fitting has been prepared for test as illustrated in Figure 4.54.



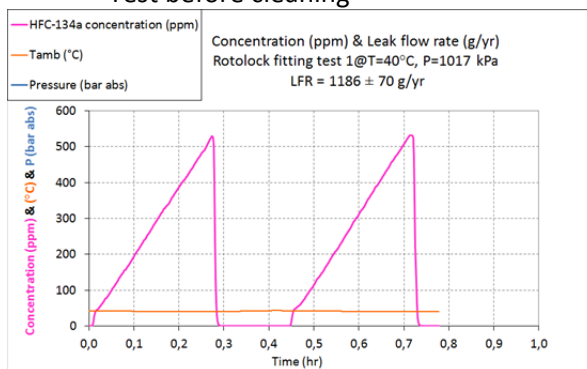
Figure 4.54: Prepared service valve n°1.



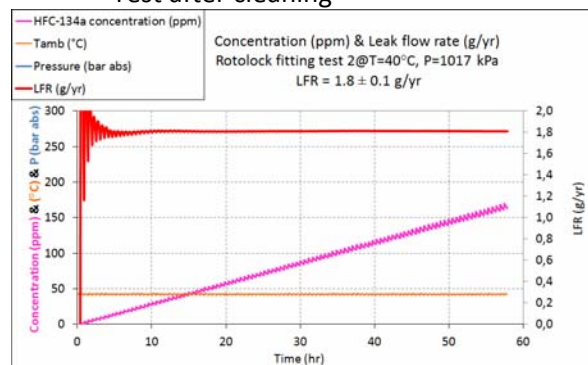
Figure 4.55: Rotolock fitting after cleaning.

This fitting has been first tested before cleaning each part. Concentration measurements presented in figures below show that the concentration increases rapidly and reaches above 500 ppm at the end of each 15-minute test. The calculated leak flow rate is 1186 g/yr. Then, both parts have been cleaned and the Teflon has been replaced by a new one. Test after cleaning leads to a LFR of 1.8 g/yr.

- Test before cleaning



- Test after cleaning



As detailed in Table 4.22, the surface roughness plays an important role on leak tightness of fittings. By cleaning the fitting, the leak flow rate reduces from 1186 to 1.8 g/yr.

Table 4.22: LFRs of Rotolock fittings.

Rotolock fitting	T [°C]	Pressure[kPa]	Leak Flow Rate [g/yr]
Before cleaning	50	1318	1186
After cleaning	50	1318	1.8

4.12 Capillary hoses

Except for the copper capillary tube, plastic capillary hoses are used to connect pressure switches to the system. A picture of tested plastic capillary hoses is shown Figure 4.56.



Figure 4.56: Plastic capillary hose.



Figure 4.57: Cut away.

From inside to outside, three different materials composed the hose:

- Inner tube: thermoplastic polymer
- Reinforcing material: polyester braid of tensile strength with modulus
- Cover material: thermoplastic polymer

Table 4.23: LFRs of plastic capillary hoses.

T [°C]	Pressure [kPa]	Leak Flow Rate [g/yr] L = 500 mm	Leak Flow Rate per meter [g/yr]
50	1318	0.15	0.30
40	1017	0.08	0.16

Based on the real length of the hose sample, the leak flow rate per meter can be easily calculated; they are 0.30 g/yr at 50°C and 0.16 g/yr at 40°C. Knowing the total length of the capillary hose used in the system, its contribution can be obtained.

4.13 Pressure switches

The pressure switch n°1 (see Figure 4.58), equipped a ¼ in female flare fitting, is connected to the refrigeration system by a Schrader valve. Pressure switch n°2, shown by Figure 4.59, is connected to the system using capillary tube.



Figure 4.58: Pressure switch n°1.



Figure 4.59: Pressure switch n°2.

Detailed measurements are shown in Appendix 2. As shown in Table 4.24, the leak flow rates of both switches are quite low: 0.003 and 0.002 g/yr. Results are very close to leakage of a flare fitting.

Table 4.24: LFRs of pressure switches.

Pressure switch	T [°C]	Pressure [kPa]	Leak Flow Rate [g/yr]
n°1	50	1318	0.003
n°2	50	1318	0.002

4.14 Summary of test results

About 50 tests have been performed to investigate the leakage level of the different components (13 types) of refrigeration systems. Table 4.25 summarizes the test results.

Table 4.25: Summary of test results.

Test description	LFR (g/yr)			
	50°C	40°C	30°C	Huge LFRs
Schrader n°1	1,08	0,69	0,41	
Solenoid valve n°1	0,165	0,086	0,047	
Solenoid valve n°2	0,165	0,086	0,04	
Solenoid valve n°3	0,23	0,15	0,07	
Solenoid valve n°4	1,31	0,82	0,44	
Flare fittings 1/4 1				
Flare fittings 1/4 8 Nm	0,003			
Flare fittings 1/4 12 Nm	0,003			
Flare fittings 1/4 16 Nm	0,002			
Flare fittings 3/8 20 Nm	0,057			
Flare fittings 3/8 30 Nm	0,02			
Flare fittings 1/2 30 Nm				12,8
Flare fittings 1/2 40 Nm	0,072			
Ball valve n°1	0,018	0,013	0,008	
Ball valve n°2	0,028	0,021	0,016	
Manual shut-off valve n°1	0,04	0,03		
Manual shut-off valve n°2	0,34	0,21		
TXV n°1	0,052	0,03	0,016	
TXV n°2	0,003			395
TXV n°3	0,021	0,015		
TXV n°4	0,016	0,011		
Electrically operated expansion valve n°1	0,017	0,008		
Electrically operated expansion valve n°2	0,012	0,006		
Pressure relief valve n°1	0,02			
Pressure relief valve n°1 after pressure relief	0,03			
Pressure relief valve n°2	0,01			
Pressure relief valve n°2 after pressure relief	0,04			
Pressure relief valve n°3	0,01			
Pressure relief valve n°3 after pressure relief	0,03			
Sight glass n°1	0,001			
Sight glass n°2	0,001			
Sight glass n°3 10 Nm				240
Sight glass n°3 15 Nm				8,6
Sight glass n°3 20 Nm	0,28			
Sight glass n°3 25 Nm	0,17			
Filter n°1	0,18	0,12	0,07	
Filter n°2	0,003			
Filter n°3	0,004			
Service valve n°1	0,004			
Service valve n°2	0,002			
Service valve n°2 after opening	0,003			
Service valve n°3	0,025			
Service valve n°3 after handling	0,021			
Service valve n°4	0,017			
Service valve n°5				1186
Service valve n°4 after cleaning				1,8
Capillary hose n°1	0,15	0,08		
Pressure switch n°1		0,003		
Pressure switch n°2		0,002		

Figure 4.60 show the leak flow rate evaluation of different components.

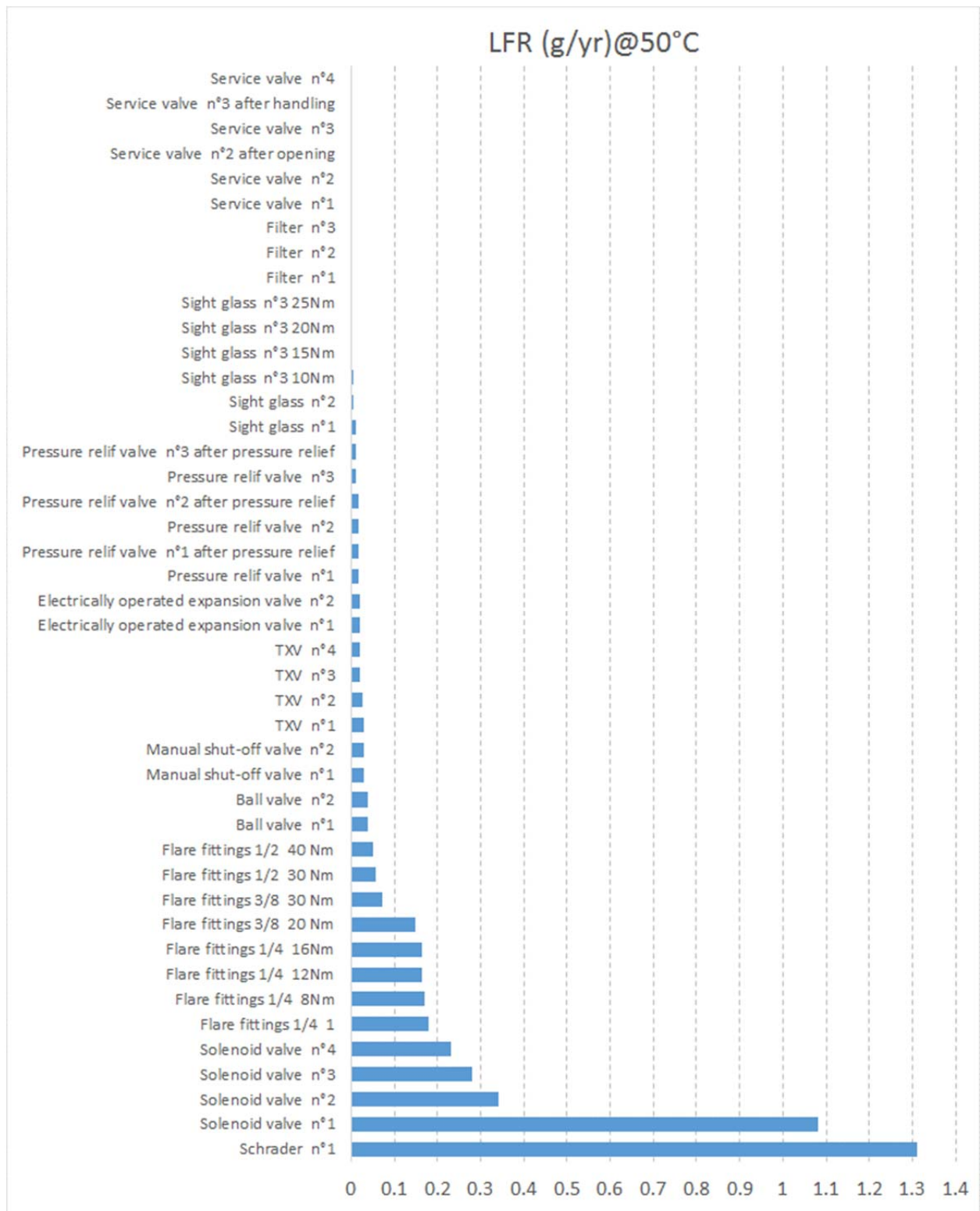


Figure 4.60: LFRs@50°C.

Several conclusions can be drawn:

- Schrader valves and solenoid valves present relatively high leak flow rates compared to other components;
- Leak flow rates of flare fittings, when tightened with the right torque, vary from 0.05 to 0.2 g/yr, but can reach very high leak flow rates when improperly tightened;
- Ball valves, manual valves, and TXVs present leakage levels in the range of 0.02 and 0.03 g/yr;
- No significant leak flow rate changes have been observed for pressure relief valves before and after pressure relief;
- Sight glasses and services valves (without Rotolock fitting) are quite leak tight;
- Hermetic components such as filters and pressure switches show good leak tightness;
- Pressure switches using flare fitting connections have very low leak flow rates (nearly non measurable)
- Very huge leakages have been observed:
 - on some valves (see Table 4.26)
 - on improperly tightened flare fittings;
 - when forgetting to mount the gasket on thermal expansion valves
 - for torque of 10 Nm or lower applied on sight glasses using Teflon O-ring
 - on improper Rotolock fittings.

Taking into account those observations, it can be concluded that

- if components are well chosen and properly mounted, the leak flow rates of refrigeration systems can be as low as some few grams / year
- but several components are by design very sensitive to improper mounting or require torque wrench.

Table 4.26 gives examples of plausible large leak flow rates.

Table 4.26: Huge leakage test results.

Tests	Leak flow rate@50°C
Flare fitting n°3 (1/2 inch) 30 Nm	12.8
TXV n°2 (without gasket)	395 g/yr
Sight glass n°3(10 Nm)	240 g/yr
Improper Rotolock fitting	1186 g/yr

Taking into account the very low leak flow rates measured on nearly all types of components, the repeatability of results did not present a significant interest because leaks coming from leak prone components can be explained based on physical causes. A larger number of tests have been performed compared to the initial commitment, because they have been seen as useful in order to explain possible causes of defaults of components such as solenoid valves and pressure relief valves.

References





- [BIVENS 2004] D. Bivens, DuPont Fluoroproducts, Private communications from supermarket chains in western and eastern United States, 2004.
- [BIRNDT 2000] R. Birndt, R. Riedel, and J. Schenk, "Tightness of Commercial Refrigeration Systems", DIE KALTE & Klimatechnik, 2000.
- [CLODIC 1998] D. Clodic. Zero leak, Ashrae, 1998.
- [CLODIC 2000] D. Clodic, "Measurement and Control of Refrigerant Leaks", AICARR Conference, 2000.
- [CLODIC 2002] D. Clodic, N. Torbey, F. Fayolle, Qualification des détecteurs de fuite – Etalonnages des fuites calibrées, in Colloque à effet de Serre III, 2002.
- [CLODIC 2004] D. Clodic, A. Zoughaib. Measurement of leak flow rates of MAC components by infra-red spectrophotometry, and calculation of annual leak flow rates, In: Proceedings of VDA alternate refrigerants winter meeting, Saalfelden, Austria, 18-19, February 2004.
- [CLODIC 2006] Clodic D. Mesure des performances de détecteurs manuels de HFC selon la norme E 35-422. MAD L'Outil Froid, mai 2000, n° 21. pp 78-81.
- [CLODIC 2006] D. Clodic, Y. Yu. Research study on the definition of the implementation of a method of measurement of annual leak flow rates (LFRs) of MAC systems ACEA /ARMINES Contract - January 2006.
- [CLODIC 2007] Y. Yu, D. Clodic. Measurements of leak flow rates of Mobile air conditioning (MAC) components - How to reach a generic approach. Dans - - SAE World Congress & Exhibition, USA (2007).
- [CLODIC 2008] Clodic D. Saba S., Slim R., Palandre L. Inventory of Direct and Indirect GHG Emissions from Stationary Air Conditioning and Refrigeration Sources, with Special Emphasis on Retail Food Refrigeration and Unitary Air Conditioning CARB Agreement No. 06-325 –December 2008
- [COWAN 2010] D. Cowan et al. , REAL Zero – Reducing refrigerant emissions & leakage - feedback from the IOR Project, IOR, 2010
- [GUIDE 1993] Guide to the expression of uncertainty in measurement. ISO, Geneva, Switzerland, 1993.
- [IEA 2003] IEA Annex 26: Advanced Supermarket Refrigeration/Heat Recovery Systems, Van Baxter, Oak Ridge National Laboratory, April, 2003.
- [MALEK 1995] A. Malek, "Leak detectors : operating principle and commercial offer" (Détecteurs de fuites: Principe et offer commerciale), Revue Générale du Froid, 33-41, June 1995.
- [MORGADO 2008] I. Morgado. Design and realization of a primary and secondary leak standards for the measurement of leak flow rates of refrigerants. Thesis – MinesParisTech –Paris 2008.
- [MORGADO 2010] I. Morgado, J.-C. Legras, D. Clodic. Primary standard for the calibration of refrigerant leak flow rates Metrologia 47, 3 (2010) 135-145.




- [RALEY's 2005] E. Estberg, FMI Energy & Technical Services Conference.
- [ROSENCWAIG 1980] Rosencwaig, Photo-acoustics and photo-acoustic spectroscopy, John Wiley and Sons, 1980.
- [SCHAFER 1999] S. Schäfer, A. Miklós, P. Hess, "Photo-acoustic Spectroscopy, Theory", Encyclopedia of Spectroscopy & Spectrometry, Lindon J, Tranter G, Holmes J, Eds, 1999, pp. 1815-1822.
- [TROY 1997] E. F. Troy, "Options for Reducing Emissions from Supermarket Systems", report for U.S. Environmental Protection Agency, EPA-600/R-97-039, Washington, D.C., April 1997.
- [URAS] Photomètre – Principe de base, ABB, presentation, Automation Products GmbH Training Analytical.
- [UNPE 2011] UNEP 2010 Report of the refrigeration, air conditioning and heat pumps technical options committee Chapter 4 commercial refrigeration, MONTREAL PROTOCOL ON SUBSTANCES THAT DEplete THE OZONE LAYER, 2011
- [VECHT 2006] M. Vecht, J. Rosendhal, A photo-acoustic approach to measure refrigerant leaks rate, VDA Alternative refrigerant winter meeting, 2006.
- [YU 2008] Y. Yu. Generic approach of refrigerant HFC-134a emissions modes for Mobile Air conditioning systems, Thesis – MinesParisTech –Paris 2008.
- [YU 2010] Y. Yu, D. Clodic. Leak flow rate of MAC systems and components 1 – Laboratory tests, fleet tests and correlation factor Fuites des systèmes et composants de conditionnement d'air mobiles. International Journal of Refrigeration (2010).





Other references




- [INT 01] <http://www.vtechonline.com/pdf/VTech%20Leak%20Detection%20Methods.pdf>, 08-2012.
- [INT 02] <http://www.lacotech.com/ProductFiles/SMT-06-1001%20Rev%20A2%20%28Tech%20Note%20A%20Production%20Leak%20Testing%29.pdf>, 09-2012.
- [INT 03] <http://www.achrnews.com/articles/115576-refrigerant-leak-detection>, 09-2012.
- [INT 04] http://en.wikipedia.org/wiki/Gas_chromatography, 08-2012.
- [INT 05] <http://chemistry.tutorvista.com/analytical-chemistry/chromotography.html#>, 08-2010.
- [INT 06] <http://refrigtech.com/Product/Manuals/LeakDetectionManual.pdf>, 10-2012.
- [INT 07] <http://www.swagelok.com/downloads/webcatalogs/EN/MS-13-150.PDF>, 10-2012
- [INT 08] http://www.enalt.com/pdf/cdz/componenti/Kit_Adattatori_a_180_per_Unita_Interne.pdf

Appendix 1: List of tested components




Item	Component reference (see report)	Brand name/ model	Description	Picture	Connection type	Tests
1	Schrader valve				Braze	• Tests of new components
2	Solenoid valve n°1	Danfoss/ <i>EVR 2</i> <i>032F8056</i>	Rubber gasket seal		Braze / braze	• Tests of new components
3	Solenoid valve n°2	Danfoss/ <i>EVR 2</i> <i>032 F 1201</i>	Rubber gasket seal		Flare / flare	• Tests of new components
4	Solenoid valve n°3	EMERSON ALCO/ <i>110 RB 2 T 2</i>	Rubber O-ring seal		Braze / braze	• Tests of new components





Item	Component reference (see report)	Brand name/ model	Description	Picture	Connection type	Tests
5	Solenoid valve n°4	EMERSON ALCO/ 200 RB 6 T 5	Rubber O-ring seal		Braze/ braze	<ul style="list-style-type: none"> • Tests of new components
6	Flare fitting n°1	Flare fittings ¼ inch	Flare fittings with nuts + copper gasket		Braze	<ul style="list-style-type: none"> • Tests with a torque of 5 Nm • Tests with a torque of 8 Nm • Tests with a torque of 12 Nm • Tests with a torque of 16 Nm
7	Flare fitting n°2	Flare fittings 3/8 inch	Flare fittings with nuts + copper gasket		Flare	<ul style="list-style-type: none"> • Tests with a torque of 10 Nm • Tests with a torque of 20 Nm • Tests with a torque of 30 Nm

Item	Component reference (see report)	Brand name/ model	Description	Picture	Connection type	Tests
8	Flare fitting n°3	Flare fittings 1/2 inch	Flare fittings with nuts + copper gasket		Flare	<ul style="list-style-type: none"> • Tests with a torque of 20 Nm • Tests with a torque of 30 Nm • Tests with a torque of 40 Nm
9	Ball valve n°1	Danfoss/ GBC 6S	Double O-ring seal PTFE ball seat		Braze/ braze	<ul style="list-style-type: none"> • Tests of new components
10	Ball valve n°1	Danfoss/ GBC 6S	Valve without Scharder fittings		Braze/ braze	<ul style="list-style-type: none"> • Tests of new components
11	Manuel shut-off valve n°1	Danfoss/ BML 6s	Stainless made diaphragm sealing		Braze/ braze	<ul style="list-style-type: none"> • Tests of new components




Item	Component reference (see report)	Brand name/ model	Description	Picture	Connection type	Tests
12	Manuel shut-off valve n°2	Castel/ 6212/2			Flare / flare	<ul style="list-style-type: none"> • Tests of new components
13	Thermo expansion valve n°1	EMERSON ALCO/ TCLE	Interchangeable thermostatic element with gasket joint		Braze/ braze	<ul style="list-style-type: none"> • Tests of new components
14	Thermo expansion valve n°2	EMERSON ALCO/ TI HW	Interchangeable thermostatic element		Braze/ braze	<ul style="list-style-type: none"> • Tests of new components





Item	Component reference (see report)	Brand name/ model	Description	Picture	Connection type	Tests
15	Thermo expansion valve n°3	Danfoss/ <i>TN 2-N</i>	One body O-ring seal for external adjustment		Flare / flare	• Tests of new components
16	Thermo expansion valve n°4	Danfoss/ <i>TCAE-N</i>	Interchangeable thermostatic element		Braze/ braze	• Tests of new components
17	Electrically operated expansion valve n°1	Castel/ <i>E2V05BSF00</i>			Braze/ braze	• Tests of new components

Item	Component reference (see report)	Brand name/ model	Description	Picture	Connection type	Tests
18	Electrically operated expansion valve n°1	Danfoss/ AKV 10-1			Braze/ braze	<ul style="list-style-type: none"> • Tests of new components
19	Pressure relief valve n°1	FAVRE/ FACR/01-14			NPT	<ul style="list-style-type: none"> • Tests of new components • Tests after 10 times relief •
20	Pressure relief valve n°2	CASTEL/ 3060/45C			NPT	<ul style="list-style-type: none"> • Tests of new components • Tests after 10 times relief

Item	Component reference (see report)	Brand name/ model	Description	Picture	Connection type	Tests
21	Pressure relief valve n°3	Danfoss/ SFA 15			NPT	<ul style="list-style-type: none"> • Tests of new components • Tests after 10 times relief
22	Sight glass n°1	Danfoss/ SGN+ 6	Sight glass with flare ends		Flare / flare	<ul style="list-style-type: none"> • Tests of new components
23	Sight glass n°2	Danfoss/ SGN+ 6s	Sight glass with brazing ends		Braze/ braze	<ul style="list-style-type: none"> • Tests of new components
24	Sight glass n°3	Carly/ VCYLS 5	Gasket sealed sight glass		braze	<ul style="list-style-type: none"> • Tests with a torque of 10 Nm • Tests with a torque of 15 Nm • Tests with a torque of 20 Nm • Tests with a torque of 25 Nm

Item	Component reference (see report)	Brand name/ model	Description	Picture	Connection type	Tests
25	Filter n°1	Carly / <i>FILTRY 3S</i>	Gasket sealed filter		Braze/ braze	• Tests of new components
26	Filter n°2	Danfoss/ <i>DCL 032</i>	One body		Flare / flare	• Tests of new components
27	Filter n°3	Parker SPORLAN/ <i>Catch all C032</i>	One body		Flare / flare	• Tests of new components
28	Service valve n°1	Castel/ 6110/22	Angle type service valve with 4 gaskets joints		¼ NPT	• Tests of new components

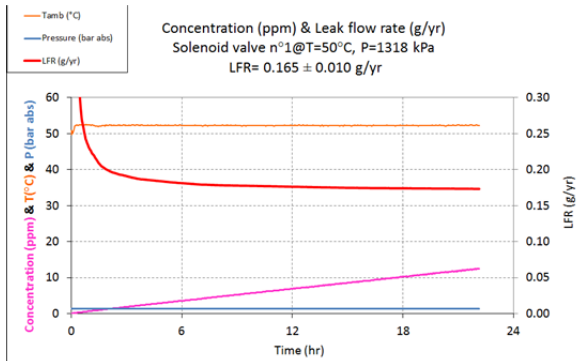
Item	Component reference (see report)	Brand name/ model	Description	Picture	Connection type	Tests
29	Angle services valves n°2	Castel/ 6420/3			Braze/ braze	<ul style="list-style-type: none"> • Tests of new components • Test after opening
30	3 ways Rotolock service valve n°3	Techmseh/	3-way compressor service valve 3/8 Teflon joint for Rotolock valve		Braze/ braze	<ul style="list-style-type: none"> • Tests of new components • Tests after handling
31	3 ways Rotolock service valve n°4	Techmseh/	3-way compressor service valve ¼ inch ¼ Teflon joints for Rotolock valve		Braze/ braze	<ul style="list-style-type: none"> • Tests of new components

Item	Component reference (see report)	Brand name/ model	Description	Picture	Connection type	Tests
32	Rotolock fitting n°5		1/2 Teflon joints for Rotolock valve		Braze/ braze	<ul style="list-style-type: none"> • Tests before cleaning • Tests after cleaning
33	Capillary hose	GOMAX/ QUADRA			Flare	<ul style="list-style-type: none"> • Tests of new components
34	Pressure switch n°1	JOHNSON CONTROLS/ P100AP-300D			Braze	<ul style="list-style-type: none"> • Tests of new components
35	Pressure switch n°2	Danfoss/ KP-1			Flare	<ul style="list-style-type: none"> • Tests of new components

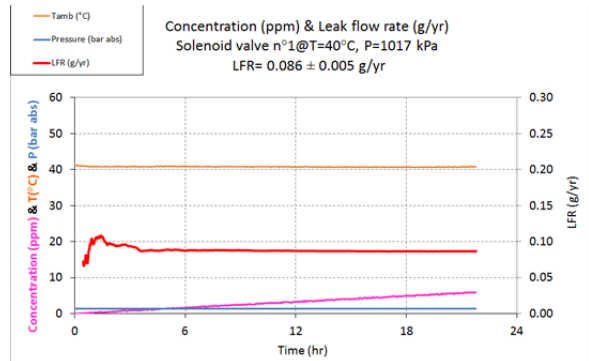
Appendix 2: LFR measurements

A.1. LFR measurement of Solenoid valve n°1:

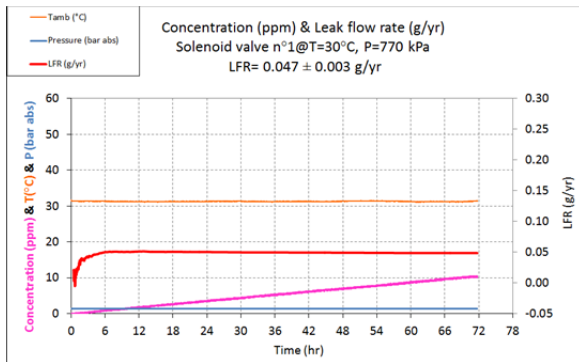
• T=50°C



• T=40°C

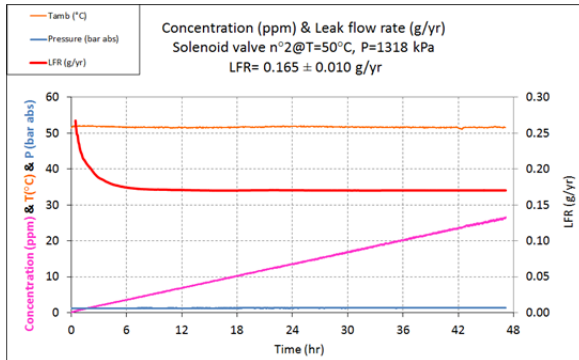


• T=30°C

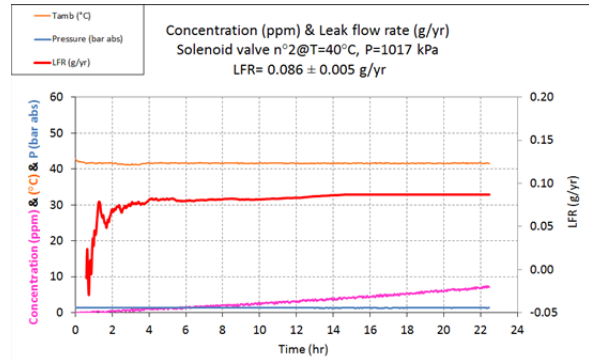


A.2. LFR measurement of Solenoid valve n°2

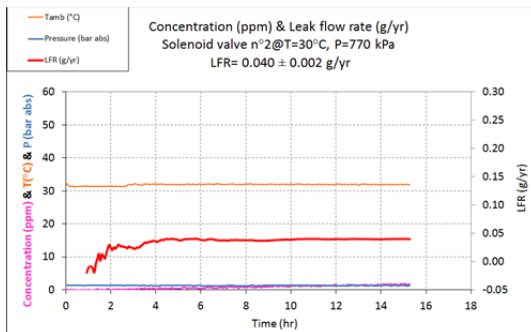
• T=50°C



• T=40°C

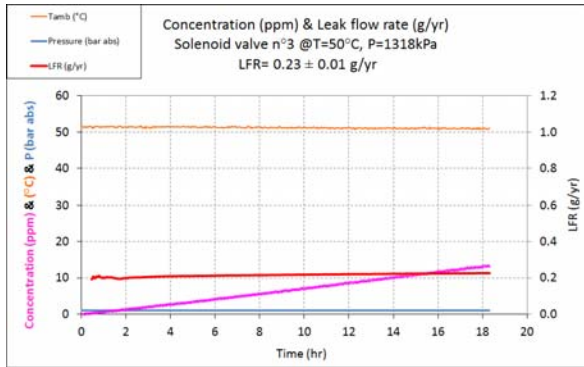


• T=30°C

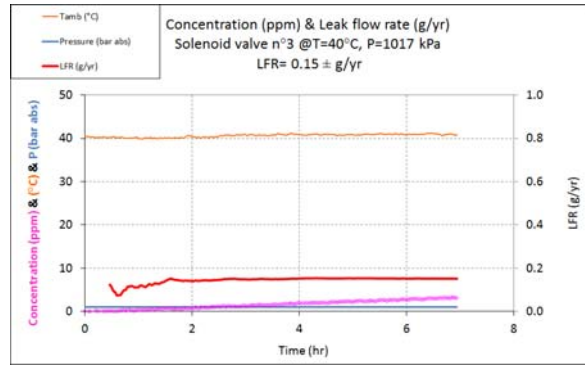


A.3. LFR measurement of Solenoid valve n°3:

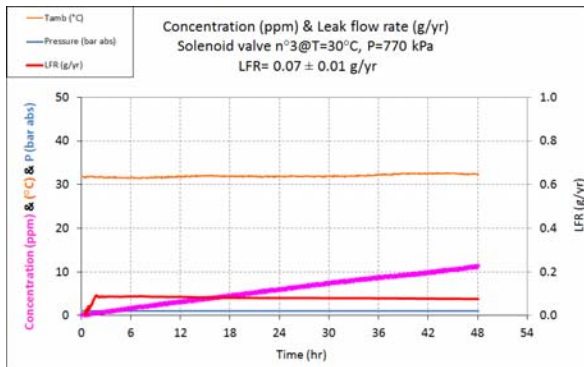
- n°1: T=50°C



- n°2: T=40°C

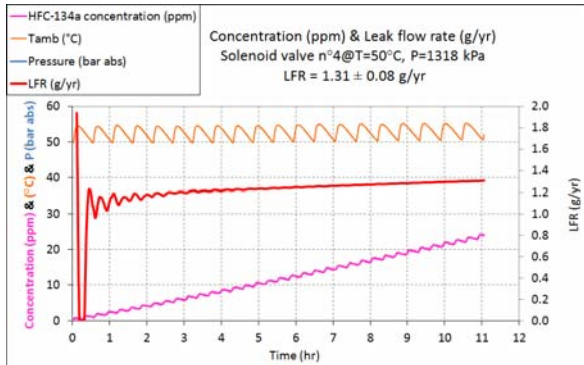


- n°3: T=30°C

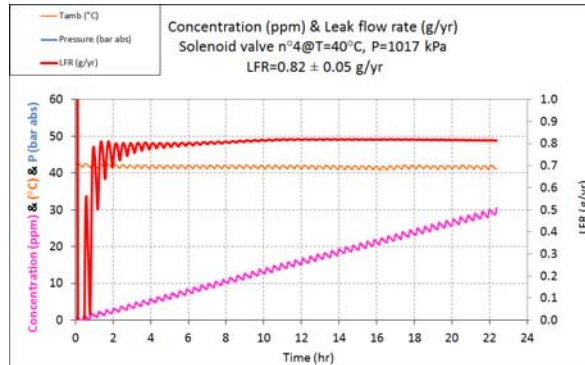


A.4. LFR measurement of Solenoid valve n°4:

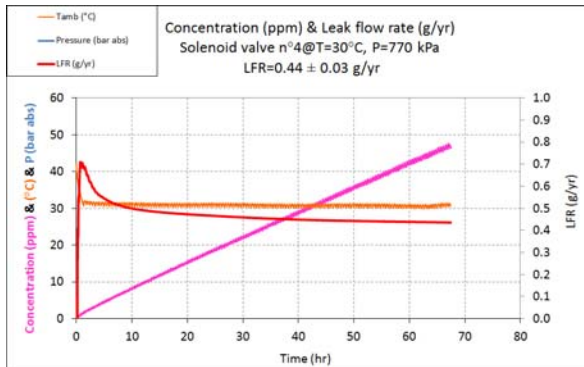
- n°1: T=50°C



- n°2: T=40°C

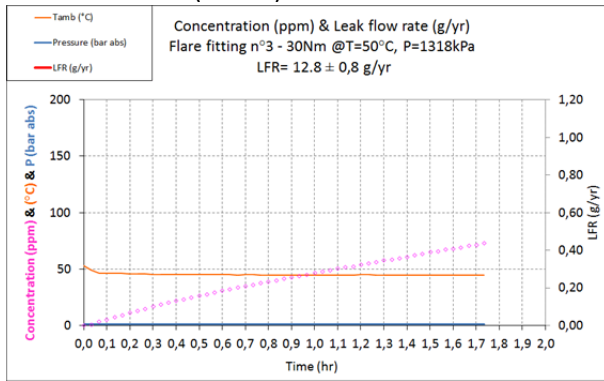


- n°3: T=30°C

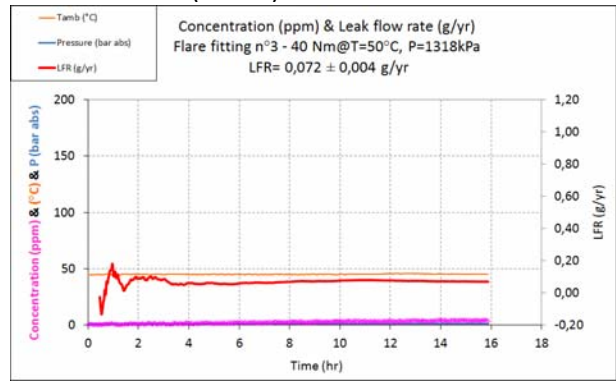


A.5. LFR measurement of Flare fitting n°3

- T=50°C (30Nm)

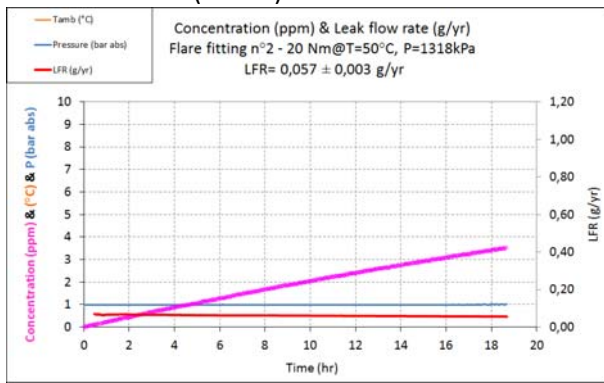


- T=50°C(40Nm)

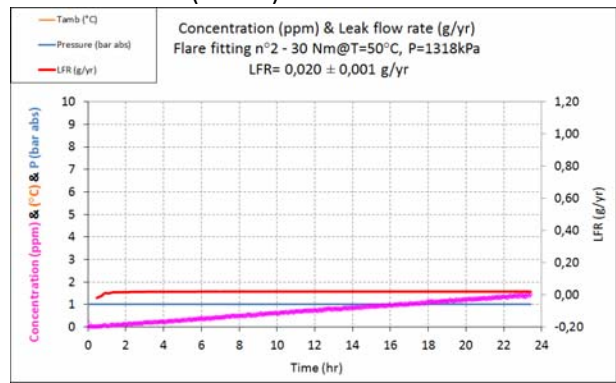


A.6. LFR measurement of Flare fitting n°4

- T=50°C (30Nm)

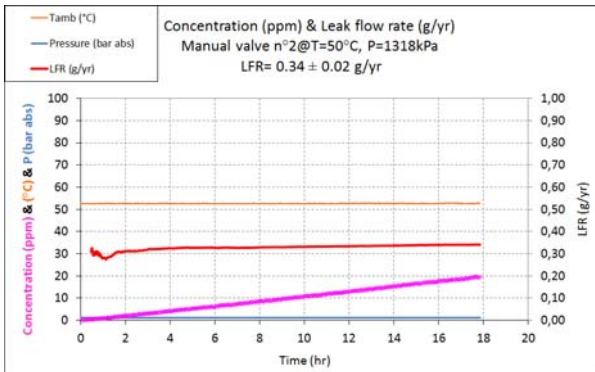


- T=50°C(40Nm)

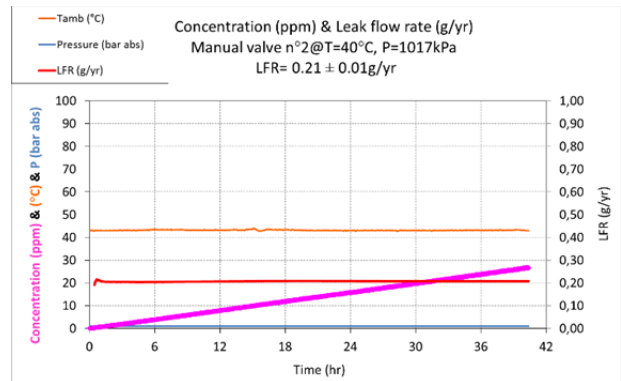


A.7. LFR measurement of manual shut-off valve n°2

- n°1:T=50°C

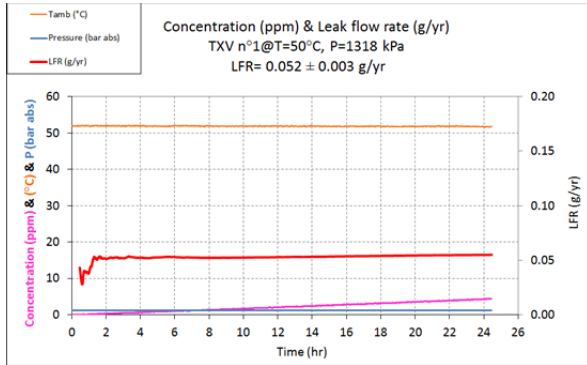


- n°2:T=40°C

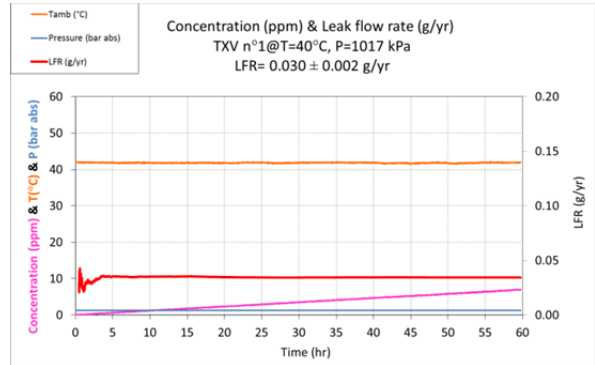


A.8. LFR measurement of TXV n°1

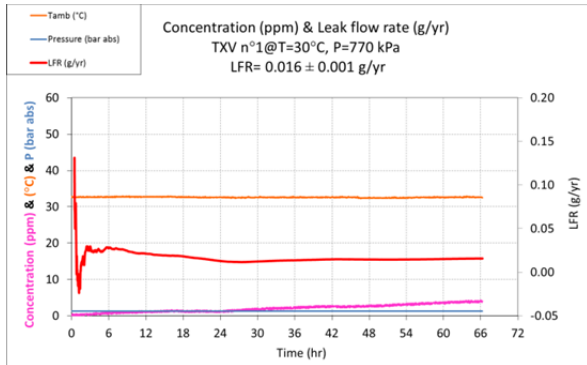
- T=50°C



- T=40°C

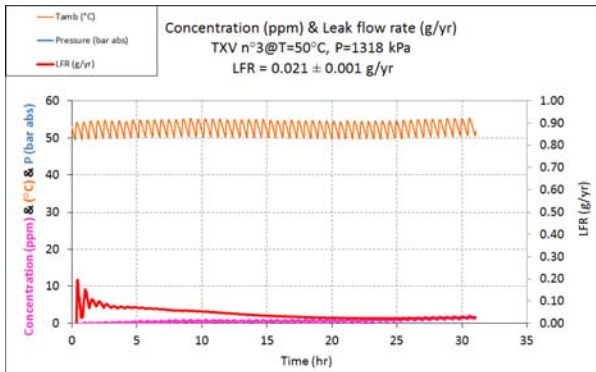


- T=30°C

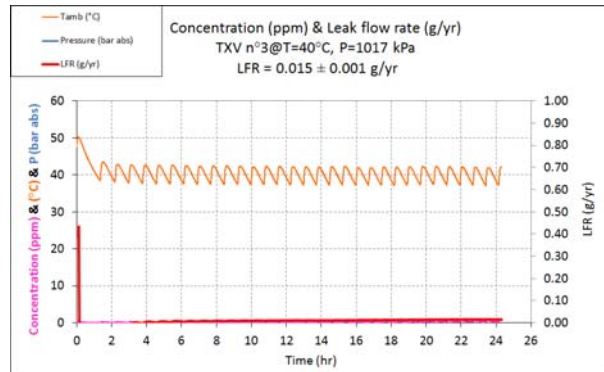


A.9. LFR measurement of TXV n°3

- n°1:T=50°C

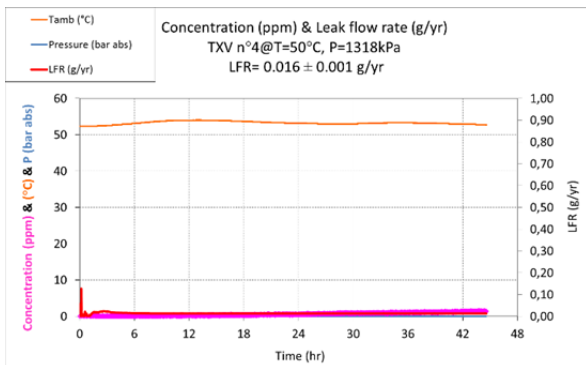


- n°2:T=40°C



A.10. LFR measurement of TXV n°4

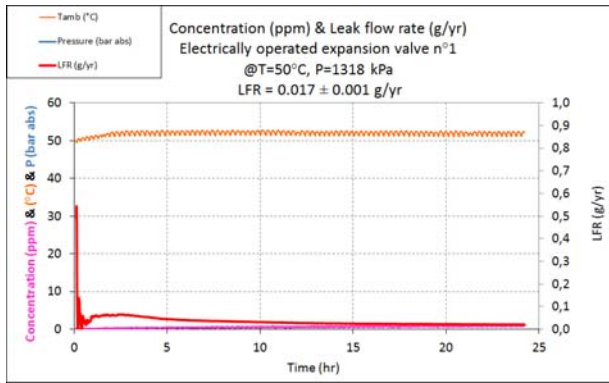
- n°1:T=50°C



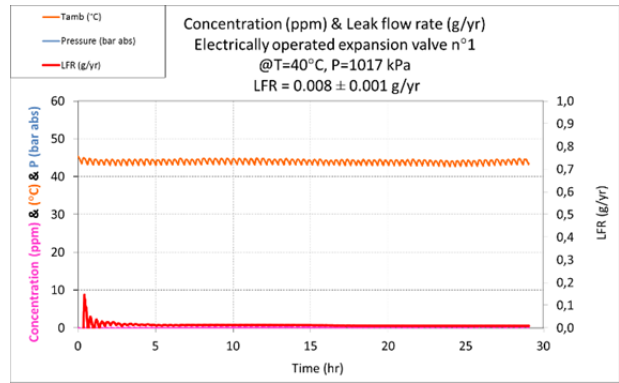
- n°2:T=40°C

A.11. LFR measurement of electrically operated expansion valve n°1

• T=50°C

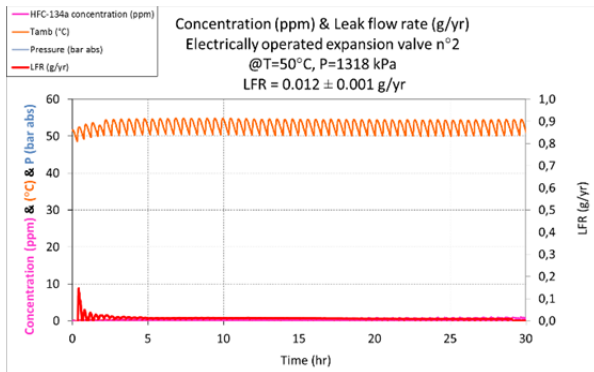


• T=40°C

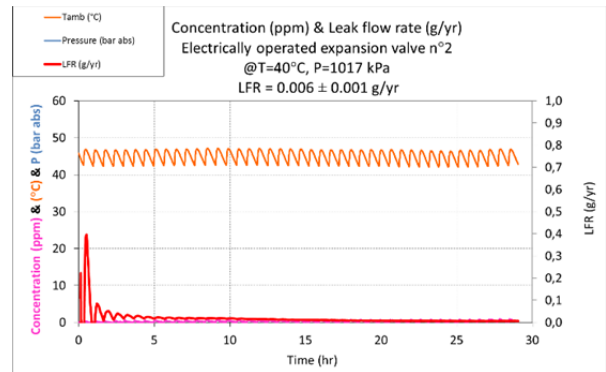


A.12. LFR measurement of electrically operated expansion valve n°2

• T=50°C

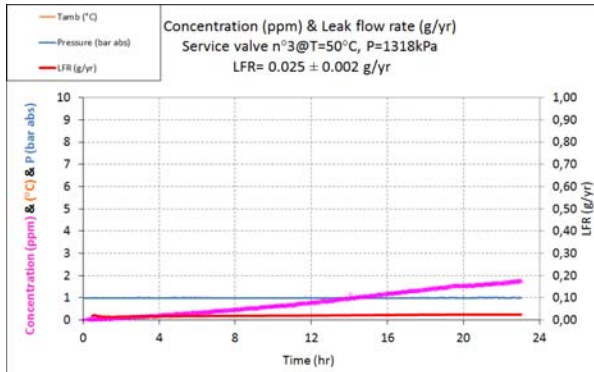


• T=40°C

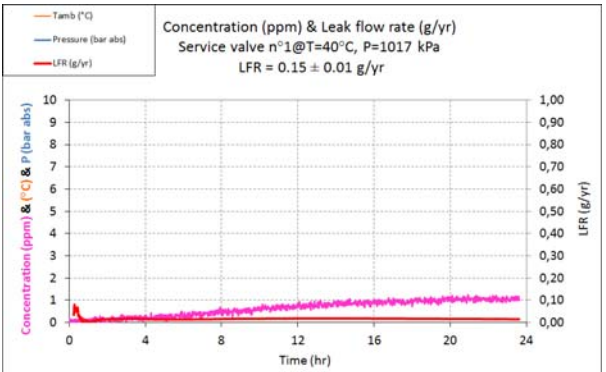


A.13. LFR measurement of service valve n°3

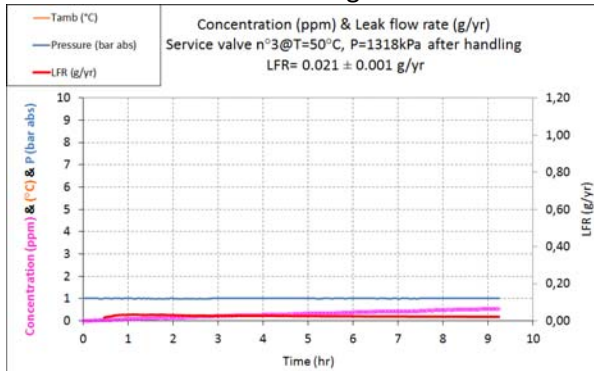
• T=50°C



• T=40°C

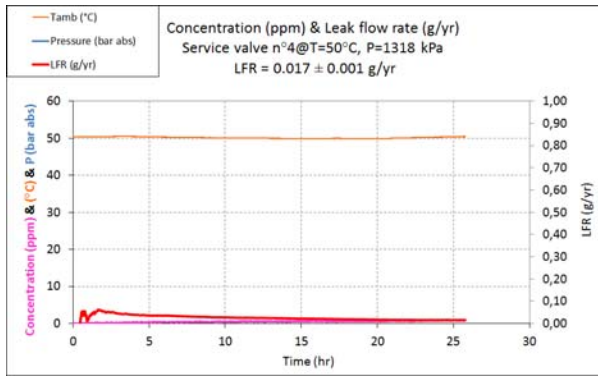


• T=50°C after handling

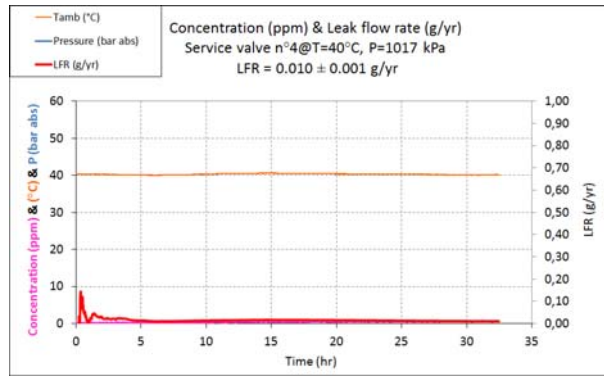


A.14. LFR measurement of Service valve n°4

- T=50°C

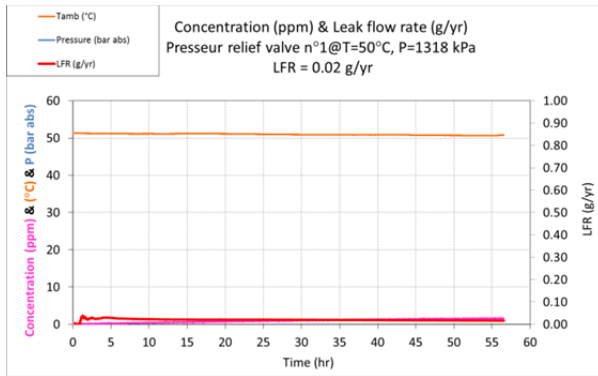


- T=40°C

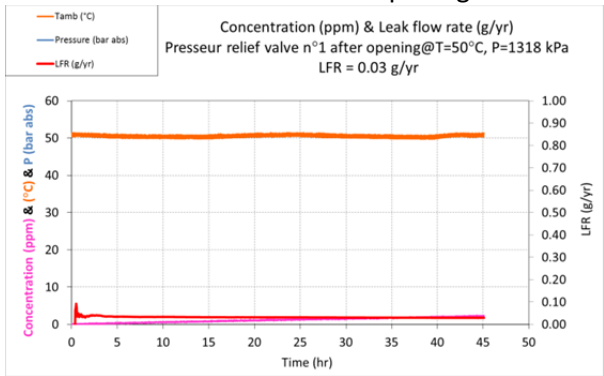


A.15. LFR measurement of Pressure relief valve n°1

- T=50°C

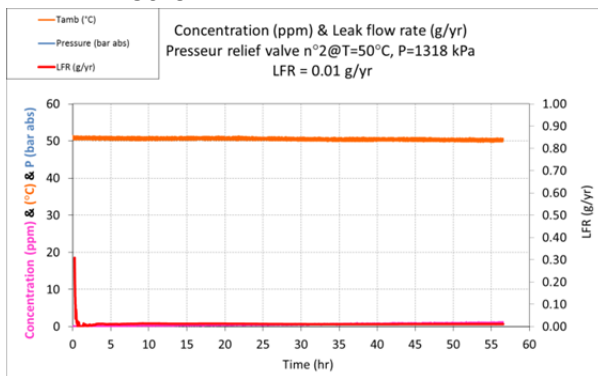


- T=50°C after 10 times' opening

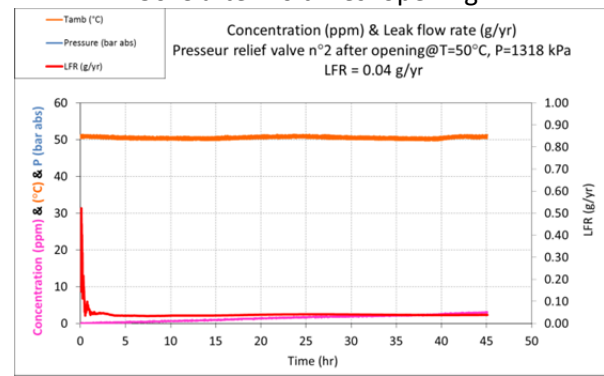


A.16. LFR measurement of Pressure relief valve n°2

- T=50°C

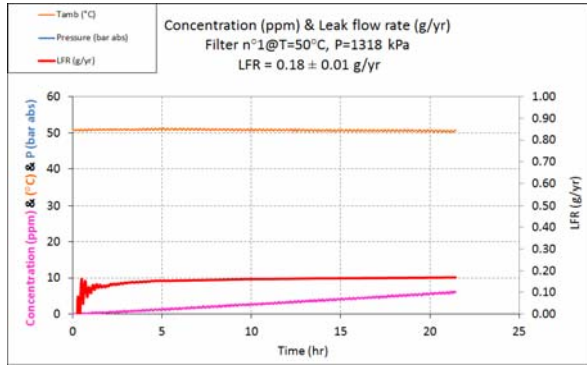


- T=50°C after 10 times' opening

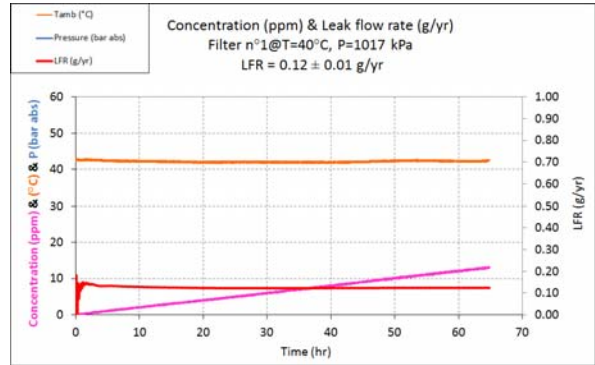


A.17. LFR measurement of filters n°4:

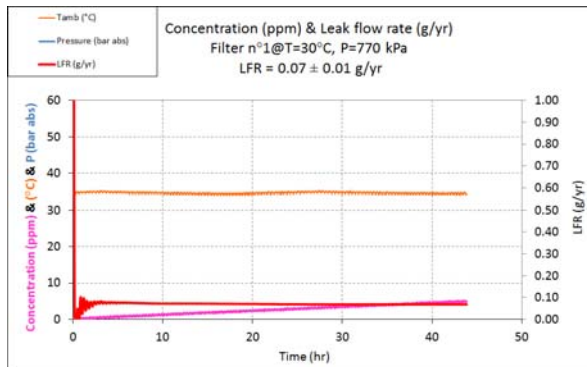
• T=50°C



• T=40°C

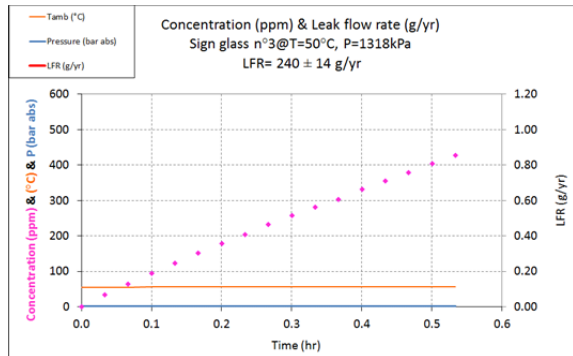


• T=30°C

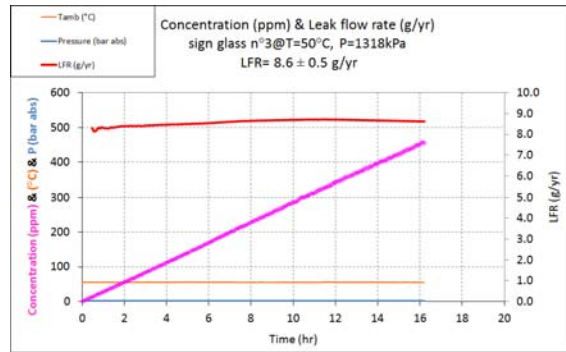


A.18. LFR measurement of sight glass n°3 (torques : 10, 15, 20 and 25Nm):

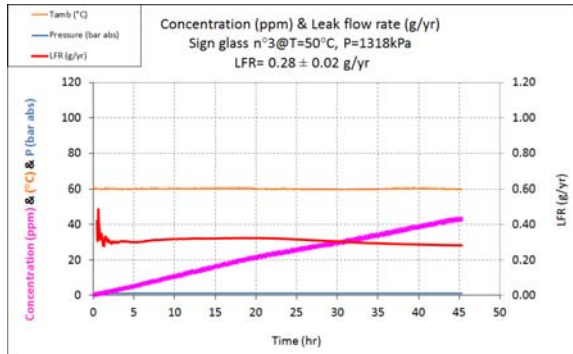
• n°1:T=50°C 10Nm



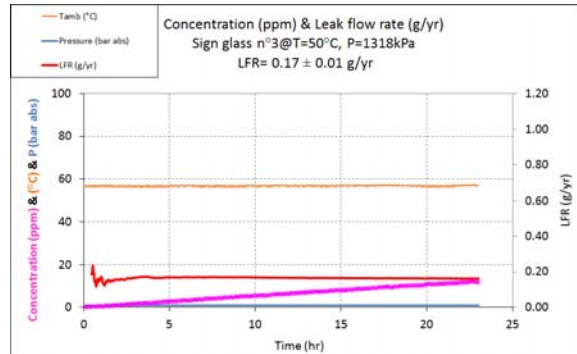
• n°2:T=50°C 15Nm



• n°3:T=50°C 20Nm

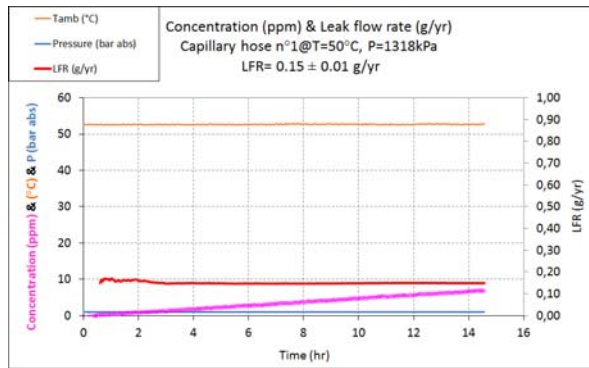


• n°4:T=50°C 25Nm

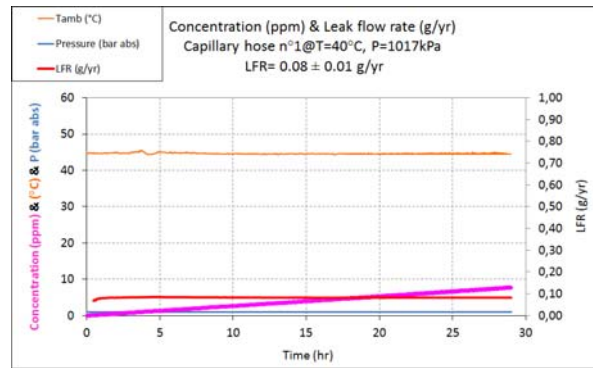


A.19. LFR measurement of capillary hose

- T=50°C

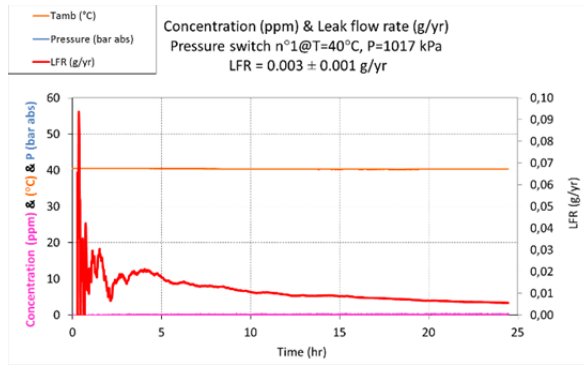


- T=40°C



A.20. LFR measurement of pressure switches n°1 and n°2

- n°1:T=40°C



- n°2:T=40°C

